Rheological and Dielectric Behavior of a Styrene−Isoprene−Styrene Triblock Copolymer in Selective Solvents. 2. Contribution of Loop-Type Middle Blocks to Elasticity and Plasticity

Hiroshi Watanabe,* Tomohiro Sato, and Kunihiro Osaki

Institute for Chemical Research, Kyoto University, Uji, Kyoto 611, Japan

Ming-Long Yao and Atsuko Yamagishi

Rheometric Scientific, F. E., 2-19-6 Yanagibashi, Taito-ku, Tokyo 111, Japan

Received December 3, 1996; Revised Manuscript Received June 6, 1997[⊗]

ABSTRACT: Rheological and dielectric behavior was examined for concentrated solutions of a styrene−isoprene−styrene (SIS) triblock copolymer in monomeric and polymeric I-selective solvents, *n*-tetradecane (C_{14}) and a low-*M* homopolyisoprene (I-1; $M = 1.4$K). The I blocks had symmetrically once-inverted dipoles along the block contour, and their midpoint motion was dielectrically detected. The SIS solutions exhibited rubbery, plastic, and viscous behavior at low, intermediate, and high temperatures (*T*). Dielectric and viscoelastic data strongly suggested that the S and I blocks were more or less homogeneously mixed in the viscous regime. In the rubbery and plastic regimes, the S blocks were segregated to form spherical domains, and the I blocks took either the loop or bridge conformation. In these regimes, the inverted dipoles of the I blocks enabled us to dielectrically estimate the loop fraction, $\phi_1 \cong 60\%$ in C_{14} and I-1. These loops, having osmotically constrained conformations, strongly affected the rheological properties of the SIS solutions. A strong osmotic constraint in C_{14} resulted in almost equal contributions of the loops and bridges to the equilibrium modulus. The loop contribution became less significant in I-1 that (partly) screened this constraint. Similarly, the yield stress σ_y in C_{14} was essentially determined by dangling (noninterdigitated) loops at relatively high *T* where the S/I mixing barrier was rather small, while the bridges and interdigitated loops had a large contribution when this barrier was enhanced, i.e., at lower *T* and/or in I-1 (a poorer solvent for the S blocks than C_{14}).

I. Introduction

Styrene−diene−styrene triblock copolymers, typical thermoplastic elastomers, offer a rich field in rheology. Those copolymers often exhibit an elastic (rubbery) response at low temperatures (*T*) while a viscous response at sufficiently high *T*.[1−6] The viscous response is usually attributed to a disordered structure (mixing) of the constituent blocks at high *T*, while the rubbery response is due to a network of glassy, discrete S domains bridged by the middle diene blocks.

In addition to these well-known responses, plastic behavior was found at intermediate *T* for a styrene−butadiene−styrene (SBS) copolymer in a B-selective solvent, *n*-tetradecane (C_{14}).[7] This plasticity was attributed to pull-out of the S blocks from softened S domains (at $T > T_g^{PS}$) due to tension of strained B blocks.[7] The S block pulled out from one domain has to experience enthalpically unfavorable contacts with B/C_{14} segments before it hops into another S domain. Thus, the flow takes place plastically, i.e., only for large stresses overwhelming this enthalpic barrier. For this mechanism of plasticity, the yield stress is determined by the mixing enthalpy of the S and B/C_{14} segments.

Recently, we investigated rheological and dielectric properties of a symmetrical styrene−isoprene−styrene (SIS) triblock copolymer in C_{14} (an I-selective solvent) to examine the above molecular pictures for the rubbery, plastic, and viscous behavior.[8] The middle I block of this copolymer had dipoles aligned without inversion along the chain contour. Those dipoles enabled us to dielectrically detect the motion of the I-block ends (end-to-end vector fluctuation). Comparison of the dielectric and rheological data revealed the following features.[8]

In the viscous regime at high *T*, the SIS/C_{14} system exhibited a significant dielectric dispersion similar to that of homopolyisoprene.[8] This result indicates that the motion of the I block ends is (almost) free from constraint due to S domains and thus the S blocks are more or less homogeneously mixed with the I blocks, as considered in the above molecular picture. On the other hand, the system exhibited no detectable dispersion in the rubbery regime at low T ($< T_g^{PS}$).[8] This fact means that the I block ends are rigidly fixed on the glassy S domains and the I blocks act as elastic strands chemically bridging the S domains, giving a support for the molecular picture. (Note, however, that only a fraction of the I blocks acts as the bridges; see the later explanation.)

For the SIS/C_{14} system in a quiescent state, no dielectric dispersion was observed at the low-*T* side in the plastic regime while the dispersion began to emerge at the high-*T* side.[8] Within the context of the above molecular picture, the I blocks hardly pull out the S blocks in the quiescent state and the motion of the I block ends is mostly limited within the S/I interface. The dispersion in the plastic regime, partly attributable to this motion, is not contradicting to the molecular picture.

However, dielectric behavior *under flow* suggested a necessity of refining the molecular picture for the plasticity: When an I block pulls out an S block from an S domain under flow, the I block ends should acquire a large motional freedom to exhibit dielectric dispersion (at frequencies corresponding to a rate of hopping of the pulled-out S block into the other S domains.) Nevertheless, no detectable flow-induced dispersion was found.[8]

[⊗] Abstract published in *Advance ACS Abstracts,* September 1, 1997.

S0024-9297(96)01757-3 CCC: $14.00

An important factor that may result in this lack of the flow-induced dispersion is the heterogeneity in the flow/deformation profile.[8] Quiescently ordered (nonaligned) block copolymer systems usually have multigrain structures with many defects.[9−12] Those systems tend to flow mostly at the grain boundaries. Thus, in our SIS/C_{14} system, only the I blocks involved in the grain boundary region would have pulled out the S blocks to exhibit dielectric activity under flow. Since those I blocks have a small population in the whole system, the flow-induced dispersion may have possessed too small intensities to be detected.

The other important factor is the I block conformation.[8] The I block of the SIS copolymer can take either a bridge conformation connecting different S domains or a loop conformation having two ends anchored on the same S domain. The bridges in the grain boundary region would be largely stretched by the applied shear and pull out the S blocks, while the (noninterdigitated) loops would be stretched much less significantly and hardly pull out the S blocks. Thus, the flow cannot induce significant dielectric changes if a large fraction of the I blocks has the loop conformation.

On the basis of the above background, this paper further investigates the molecular origins of the rubbery (elastic), plastic, and viscous behavior of the SIS/C_{14} system, placing its focus on the contribution of the loop-type I blocks to the elasticity and plasticity. We use a specially designed SIS copolymer having dipole inversion at the midpoint of the I blocks. This inversion enables us to dielectrically detect the midpoint motion and estimate the loop fraction. Furthermore, following a strategy of previous studies[13−15] for plasticity of diblock copolymer micelles, we compare rheological behavior of the SIS copolymer in C_{14} and a low-M homopolyisoprene (hI): The loops in C_{14} can exhibit the elasticity and plasticity with a molecular origin identical to that for the micellar corona blocks, an osmotic constraint for the block conformation.[13−15] In hI, this constraint should be reduced[14] and the loop contribution should be decreased. On the other hand, the bridges exhibit the elasticity in both C_{14} and hI, and their plasticity is determined by the enthalpic barrier for mixing of the S and I blocks. This barrier should be larger in hI than in C_{14} and the bridge contribution to the plasticity should be enhanced in hI. On the basis of these ideas, we compare the equilibrium moduli and yield stresses for the SIS chains in C_{14} and hI to examine the loops and bridge contributions to these quantities.

II. Experimental Section

II.1. Materials. A styrene−isoprene−styrene triblock copolymer having symmetrically *once-inverted* dipoles in the I block was used. In the remaining part of this paper, we designate this sample as SIIS (instead of a commonly used abbreviation, SIS), emphasizing its dipole inversion. The SIIS sample was synthesized with a previously used method:[16,17] First, SI^-Li^+ diblock anions were polymerized with *sec*-butyllithium in benzene. A fraction of these anions were terminated with methanol to obtain the SI sample having the dipoles aligned in the same direction along the I block contour. The remaining anions were coupled at the I block ends with a prescribed amount (≅95% equimolar) of *p*-xylyrene dichloride, and a small amount of unreacted SI precursors was thoroughly removed by fractionation from the benzene/methanol mixture to recover the SIIS sample. Molecular characteristics of these SI and SIIS samples are summarized in Table 1. The molecular weights M were evaluated from the S content (28.7 wt %; determined from H-NMR) and M of their S precursor (7.2K; determined from GPC).

Table 1. Characteristics of Samples[a]

code	$10^{-3}M$ for block sequence	$10^{-3}M^b$	M_w/M_n[c]
SI 7-18	7.2−17.9	25.1[d]	1.07
SIIS 7-18-18-7	7.2−17.9−17.9−7.2	50.2[d]	1.07
I-1		1.4[e]	1.10

[a] Cis/trans/vinyl ≅ 75/20/5 for I (determined from H-NMR). [b] Total molecular weight. [c] Determined from GPC. [d] Weight-average molecular weight evaluated from the S/I composition and M for precursor S. [e] Number-average molecular weight determined from H-NMR.

A low-M homopolyisoprene (designated as I-1) was used as an I-selective, polymeric solvent for SIIS and SI. I-1 was anionically synthesized with *tert*-butyllithium in benzene, and its molecular characteristics were determined from H-NMR and GPC; see Table 1. (M was determined from H-NMR by counting the proton numbers for the *tert*-butyl groups and isoprene monomer units in I-1.)

The systems subjected to rheological and dielectric tests were the SIIS solutions in I-selective, monomeric and polymeric solvents, *n*-tetradecane (C_{14}; Wako) and I-1. The SIIS concentration was 50 wt % in C_{14} and 45.3 wt % in I-1. At low T where the S blocks were strongly segregated from the I blocks, these solutions had the same I block concentration in the C_{14} and I-1 matrices (c_{bI} = 0.34 g cm^{-3}; evaluated under an assumption of volume additivity).

As explained earlier, the osmotic constraint for the I block conformation should be reduced when the solvent is switched from C_{14} to I-1. For quantifying this reduction as well as for estimating the loop fraction of SIIS, we also examined rheological and dielectric properties for solutions of the precursor SI in C_{14} and I-1. The SI concentrations in these solutions (50 wt % in C_{14} and 45.3 wt % in I-1) were identical to the SIIS concentrations explained above.

The solutions were prepared by first dissolving a prescribed amount of the copolymer (SIIS or SI) and the solvent (C_{14} or I-1) in an excess of benzene, and then allowing benzene to thoroughly evaporate. The SIIS or SI concentration in the C_{14} solutions was determined after complete evaporation of benzene. The volume fraction of the S blocks in the solutions was ≅12 vol %. As judged from structural data for similar copolymer systems having such small S content,[18,19] spherical S domains were formed in our SIIS and SI solutions in strongly segregated states (at low T): In the SIIS solutions, the S domains are interconnected by the bridge-type I blocks (coexisting with the loop-type I blocks) to form a network structure. On the other hand, the SI solutions have no network structure but contain spherical micelles with S cores and I corona, the latter having a tail conformation.

II.2. Measurements. Rheological Measurements. Dynamic measurements were carried out for the SIIS and SI solutions at T = 15−70 °C with a rheometer (RMS605, Rheometrics). The measurements were carried out with a cone-and-plate geometry, and a frictionless jacket sealed with C_{14} was used for the two C_{14} solutions to prevent changes in the SIIS and/or SI concentration. The cone diameter was 2.5 cm, and the gap angle between the cone and plate was 0.1 rad. The amplitude of the oscillatory strain, γ_0, was varied from 0.003 to 0.4. From the dynamic data for those γ_0, the rubbery, plastic, and viscous regimes were specified for the SIIS/C_{14} and SIIS/I-1 solutions (cf. Figures 1−5 shown later). For the SI/C_{14} and SI/I-1 solutions, the plastic and viscous regimes were specified. (These micellar solutions, having no network structure, exhibited no rubbery responses.)

For the SIIS/C_{14} and SIIS/I-1 solutions, creep measurements were also carried out in the rubbery and plastic regimes. The measurements were carried out with a rheometer (SR-500, Rheometrics) in a parallel plate geometry of diameter = 2.5 cm.

In the dynamic measurements with sufficiently small γ_0, linear viscoelastic responses were detected for all solutions in the entire range of T examined: The stress $\sigma(t)$ oscillated sinusoidally with time and the resulting moduli were independent of γ_0. From those responses the storage and loss moduli, G' and G'', were determined.

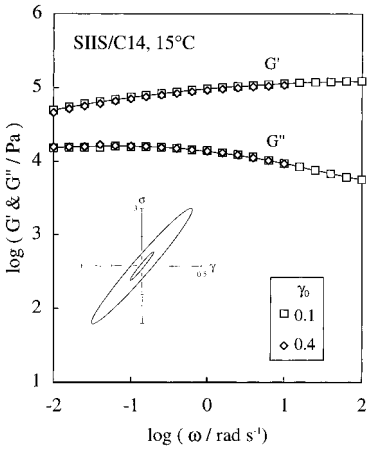

Figure 1. Linear viscoelastic moduli and typical Lissajous patterns (at $\omega = 0.1$ rad s^{-1}; σ in units of 10^4 Pa) for the SIIS/C_{14} system ($c_{SIIS} = 50$ wt %) at 15 °C. No nonlinearity is seen for $\gamma_0 \leq 0.4$.

On the other hand, for large γ_0, significant nonlinearities were observed for the solutions in the plastic regime: $\sigma(t)$ oscillated nonsinusoidally to exhibit *lozenge-shaped* Lissajous patterns ($\sigma-\gamma$ patterns; cf. Figure 2 shown later). Those $\sigma(t)$ data were Fourier-analyzed according to eq 1 to evaluate nonlinear moduli for the jth harmonics,[13] G_j' and G_j''.

$$\gamma(t) = \gamma_0 \sin \omega t,$$

$$\sigma(t) = \gamma_0 \sum_{j=\text{odd}} [G_j' \sin j\omega t + G_j'' \cos j\omega t] \quad (1)$$

In the rubbery regime, the solutions exhibited linear viscoelastic responses in the entire range of γ_0 (=0.003−0.4), and G_1' and G_1'' were reduced to the γ_0-independent linear moduli, G' and G''. The linear responses for those γ_0 were observed also at the high T side in the viscous regime. At the low T side in this regime (close to a boundary between the plastic and viscous regimes), $\sigma(t)$ was almost sinusoidal but the resulting moduli, G_1' and G_1'', were dependent on γ_0 for large γ_0 (cf. Figure 3).

Dielectric Measurements. Dielectric measurements were carried out for the SIIS and SI solutions with capacitance bridges: GR 1689A (General Radio) was used at low frequencies $\omega \leq 2 \times 10^5$ rad s^{-1}, and HP 4285A (Hewlett-Packard), at high $\omega > 2 \times 10^5$ rad s^{-1}. In the plastic and viscous regimes, the measurements under large-γ_0 oscillatory shear and steady shear were carried out with a cone-and-plate type rheo-dielectric cell mounted on a rheometer (Autoviscometer L-III, Iwamoto Seisakusho, Kyoto). Details of the cell and rheometer, the latter being modified to include a mercury reservoir for good electrical contact under shear, were shown elsewhere.[8] The measurements at the quiescent state were carried out in all regimes with the rheo-dielectric cell and a conventional cell composed of guarded, parallel plate electrodes.

Determination of T_g^{PS}. Differential scanning calorimetric measurements were carried out for the SIIS and SI chains in C_{14} and I-1 with a scanning calorimeter (DSC2910, TA Instruments) to determine T_g^{PS} of the S domains. The results were $T_g^{PS} = 30 \pm 4$ °C in C_{14} and $T_g^{PS} = 41 \pm 5$ °C in I-1, both obtained at a heating rate of 10 °C/min. These T_g^{PS} are lower than T_g of bulk PS, suggesting that the S domains are plasticized with C_{14} and/or I-1. (A small amount of the short I-1 chains ($M = 1.4$K) is mixed with the relatively short S blocks ($M = 7.2$K) even at low T.)

III. Results

III.1. Assignment of Rubbery, Plastic, and Viscous Regimes. We examined dynamic mechanical data obtained for various strain amplitudes γ_0 to assign the rubbery, plastic, and viscous regimes for the SIIS and SI copolymers in C_{14} and I-1. Typical Lissajous patterns at low ω and moduli data in respective regimes are demonstrated in Figures 1−4 for the SIIS/C_{14} system.

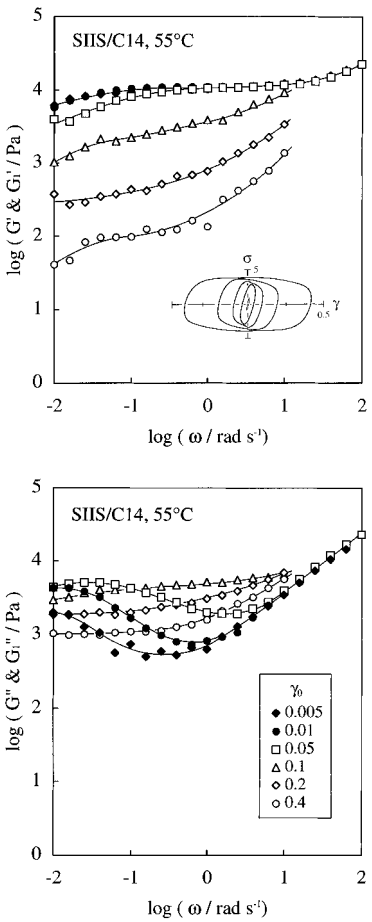

Figure 2. Nonlinear viscoelastic moduli and typical Lissajous patterns (at $\omega = 0.025$ rad s^{-1}; σ in units of 10^2 Pa) for the SIIS/C_{14} system ($c_{SIIS} = 50$ wt %) at 55 °C. For $\gamma_0 = 0.005$, the nonlinear moduli are reduced to the linear G' and G''.

At 15 °C (Figure 1), the SIIS/C_{14} system exhibits elliptic Lissajous patterns $\gamma_0 \leq 0.4$. The moduli, G' and G'', are independent of γ_0, and G' is weakly dependent on the frequency (ω) while G'' is considerably smaller than G'. This behavior is similar to that of softly cross-linked rubbers exhibiting weak relaxation at long time scales. This result enables us to assign the SIIS/C_{14} system to be in the rubbery regime at 15 °C.

At 55 °C (Figure 2), linear responses characterized with the elliptic Lissajous patterns, fairly ω-insensitive G', and considerably smaller G'' is observed for *small* γ_0 (=0.005). This behavior is similar to the rubbery behavior seen at 15 °C (Figure 1). However, Figure 2 also demonstrates that the patterns for large γ_0 are lozenge-shaped and their stress amplitudes (at low ω) are insensitive to γ_0. Correspondingly, the nonlinear moduli for the fundamental harmonics, G_1' and G_1'' (eq 1), significantly decrease with increasing $\gamma_0 > 0.05$. These nonlinear features are characteristic of plastic fluids.[8,13,15] Thus the SIIS/C_{14} system is assigned to be in the plastic regime at 55 °C.

At 60 °C (Figure 3), the Lissajous patterns are (almost) elliptic but the resulting G_1' and G_1'' are dependent on γ_0 for large γ_0 (>0.1). Despite this nonlinearity, G_1' and G_1'' strongly decrease with decreasing ω. In particular, in the linear regime ($\gamma_0 <$ 0.1), the terminal behavior ($G' \propto \omega^2$, $G'' \propto \omega$) is observed at low ω. Thus the SIIS/C_{14} system is in the nonlinear viscous regime at 60 °C.

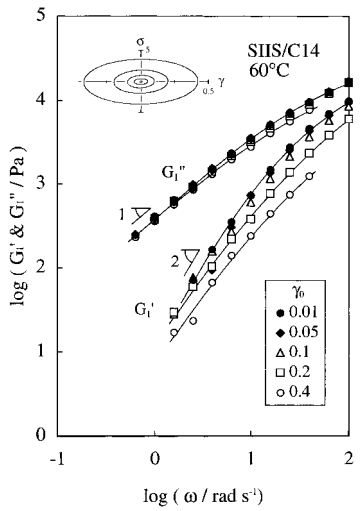

Figure 3. Nonlinear viscoelastic moduli and typical Lissajous patterns (at $\omega = 2.5$ rad s^{-1}; σ in units of 10^2 Pa) for the SIIS/C_{14} system ($c_{SIIS} = 50$ wt %) at 60 °C. For $\gamma_0 \leq 0.05$, the nonlinear moduli are reduced to the linear G' and G''.

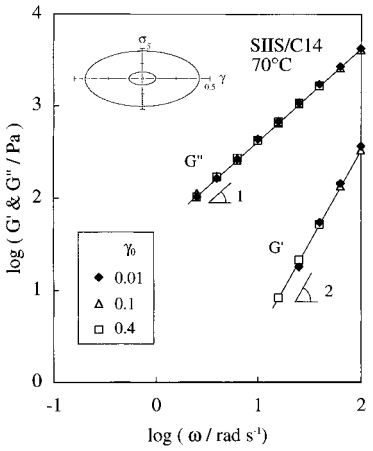

Figure 4. Linear viscoelastic moduli and typical Lissajous patterns (at $\omega = 25$ rad s^{-1}; σ in units of 10^2 Pa) for the SIIS/C_{14} system ($c_{SIIS} = 50$ wt %) at 70 °C. No nonlinearity is seen for $\gamma_0 \leq 0.4$.

Finally, at 70 °C (Figure 4), elliptic Lissajous patterns are observed in the entire γ_0 range, and the resulting moduli are independent of γ_0. Since the terminal flow behavior is seen in the entire ranges of ω and γ_0 examined, the SIIS/C_{14} system is classified to be in the linear viscous regime at 70 °C.

All four regimes explained above were found also for the SIIS/I-1 system, while no rubbery regime existed for the SI/C_{14} and SI/I-1 systems (containing no network structure). Figure 5 maps those rheological regimes for the systems examined. The filled and unfilled squares indicate that the system behaved as a viscous fluid with and without nonlinearities for large γ_0 (cf. Figures 3 and 4).

III.2. Linear Viscoelastic Behavior. For the SI and SIIS systems, Figures 6−9 show the linear moduli G' and G'' obtained for sufficiently small γ_0. These moduli have negligible contribution from the solvents (C_{14} and I-1) and exclusively represent the equilibrium behavior of SIIS and/or SI chains in respective solvents. In the strongly segregated state (at low T), all systems have the same I block concentration in the C_{14} and/or I-1 matrices ($c_{bI} = 0.34$ g cm^{-3}).

Rheological and structural properties have been extensively studied for concentrated micellar solutions of diblock copolymers in selective solvents.[13−15,19,20] Those

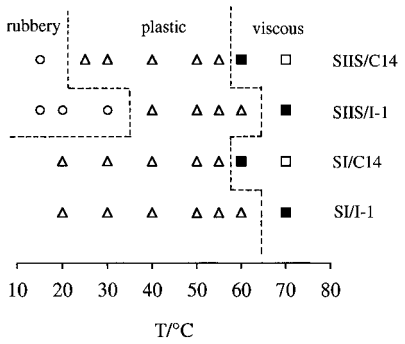

Figure 5. Map specifying the rubbery (circles), plastic (triangles), and viscous (squares) regimes for the SIIS and SI systems with the SIIS and/or SI concentration of 50 wt % (in C_{14}) and 45.3 wt % (in I-1). The filled and unfilled squares indicate that the systems behaved as a viscous fluid with and without nonlinearities for $\gamma_0 \leq 0.4$.

studies revealed that the properties of the micelles are strongly influenced by an osmotic constraint for the corona block conformation. The corona I blocks of our SI micelles are subjected to strong osmotic constraint in C_{14}, but this constraint should be reduced in the polymeric solvent, I-1.[14] This reduction becomes a key factor in our later discussion for elasticity and plasticity of SIIS systems. To quantify the reduction, this section first summarizes rheological features of our SI/C_{14} and SI/I-1 micellar systems in relation to the effect of the osmotic constraint and then describes the features of the SIIS/C_{14} and SIIS/I-1 systems.

Behavior of SI Systems. The SI/C_{14} and SI/I-1 systems exhibit qualitatively similar behavior (Figures 6 and 7): At low T, both systems behave as elastic solids (against small strain) to exhibit ω-insensitive G' and quite small G'' at low ω. In particular, at 20 °C, the systems exhibit no detectable loss at low ω (see the G''/G' *vs* ω plots). On the other hand, at high T, they behave as viscous liquids to exhibit the terminal flow behavior. Specifically, at 70 °C, the SI/C_{14} system exhibited undetectably small G' (<1 Pa) even at the highest ω examined (10^2 rad s^{-1}).

In general, concentrated spherical micelles form cubic lattices at low T[13−15,19,20] while structural transitions (lattice disordering and mixing of the constituent blocks) occur at high T.[13−15,20] The elastic response of our SI systems at low T is attributed to a restoring force of this lattice against a slow, small strain. (Viscoelastic relaxation of our corona I blocks is completed at short time scales, $\omega > 1$ rad s^{-1}.) The viscous response at high T is attributable to relaxation of the disordered lattice/blocks.

Quantitatively, the SI/C_{14} and SI/I-1 systems exhibit a difference in their equilibrium moduli G_e ($=[G']_{\omega\to 0}$) *at low T*. This modulus, representing the stability of the micellar lattice, is smaller by a factor $\cong 2$ in I-1 (Figure 7) than in C_{14} (Figure 6). This result is a natural consequence of the osmotic nature of the micellar lattice formation: In the SI/C_{14} system, the corona I blocks are required to have a uniform segment distribution in the matrix phase so as to decrease their osmotic energy.[13−15] To satisfy this requirement, these corona blocks (tethered on S cores) have to take mutually correlated, distorted conformations having small entropy. The micellar lattice is formed as the thermodynamically most stable structure that minimizes this osmotic constraint for the corona conformation.[13−15] In the SI/I-1 system, the I-1 chains (chemically identical to the corona) behave as a buffer preserving the uniform distribution of the I segments irrespective of the corona

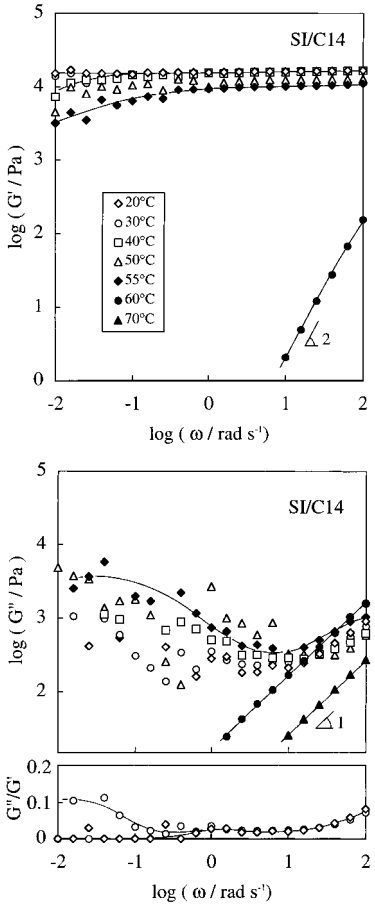

Figure 6. Linear viscoelastic moduli of the SI/C_{14} system (c_{SI} = 50 wt %) at various temperatures. At 20 °C, the system exhibits no detectable loss at low ω (see the plots of tan $\delta = G''/G'$).

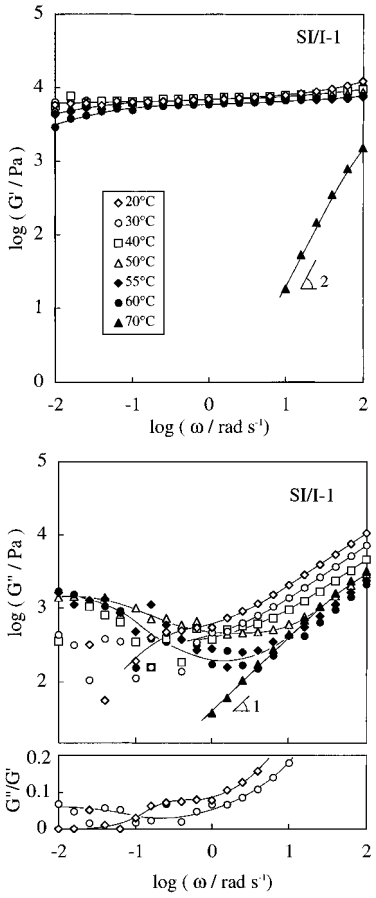

Figure 7. Linear viscoelastic moduli of the SI/I-1 system (c_{SI} = 45.3 wt %) at various temperatures. At 20 °C, the system exhibits no detectable loss at low ω (see the plots of tan $\delta = G''/G'$).

conformation.[14,15] Thus, the I-1 chains reduce the osmotic constraint, allow the corona I blocks to take randomized conformation more freely in I-1 than in C_{14}, and destabilize the lattice.[21] The difference of G_e for the SI/C_{14} and SI/I-1 systems quantifies this reduction in the I-1 matrix.

Behavior of SIIS Systems. In Figures 8 and 9, the unfilled, half-filled, and fully filled symbols indicate G' and G'' for the SIIS/C_{14} and SIIS/I-1 systems in the rubbery, plastic, and viscous regimes, respectively. The solidlike response seen in the plastic regime is the linear response before yielding. For both systems, the time−temperature superposition is invalid due to structural changes with T.

Quantitatively, the SIIS/C_{14} and SIIS/I-1 systems exhibits a difference: G' in the plastic regime is more sensitive to T for the latter system. As confirmed for the SI micellar systems, the osmotic constraint for the I block conformation is reduced in I-1. The difference between the SIIS/C_{14} and SIIS/I-1 systems, being related to this reduction, is later utilized for examining the contributions of the loop- and bridge-type I blocks to elasticity and plasticity of SIIS.

III.3. Dielectric Behavior. Figures 10−13 show the dielectric loss ϵ'' of the SIIS and SI systems at the quiescent state (filled circles). For the systems in the plastic and viscous regimes, dielectric measurements were also carried out under steady/oscillatory flow. The resulting ϵ'' data were indistinguishable from those at the quiescent state. This shear-insensitivity of ϵ'' was also found in our previous work[8] (for an SIS copolymer having no dipole inversion).

The solvent, C_{14}, had negligibly small ϵ'' at T and ω examined. Thus, in Figures 10 and 11, the ϵ'' data represent the dielectric loss of the SIIS and SI chains, ϵ''_{SIIS} and ϵ''_{SI}. On the other hand, for the SIIS/I-1 and SI/I-1 systems (Figures 12 and 13), a dispersion of the matrix I-1 chains (having parallel dipoles) is seen as the peaks or shoulders in the ϵ'' curves at $\omega > 10^5$ rad s^{-1}. For these systems, we evaluated ϵ''_{SIIS} and ϵ''_{SI} by subtracting the matrix contribution (dotted curves) from the ϵ'' data (filled circles). The ϵ''_{I-1} data of pure I-1 reduced by the I-1 content in the systems were used as this matrix contribution. The monomeric friction ζ of the short I-1 chains increased when they were mixed with much longer I blocks. This increase was compensated for by shifting the reduced ϵ''_{I-1} curve to the lower-ω side until it was superimposed on the ϵ'' curves of the SIIS and SI systems at their high-ω peaks or shoulders; see the dashed curves in Figures 12 and 13. (At respective T, the same amount of shift was achieved for the two systems as the common correction for ζ.)

For the SIIS and SI chains in I-1, the above subtraction unavoidably introduces large uncertainties in ϵ''_{SIIS} and ϵ''_{SI} at high ω. Thus, in examination of the dielectric behavior of these chains in I-1, we use the ϵ''_{SIIS} and ϵ''_{SI} data only at low ω where the uncertainties are acceptably small. Those data are shown in Figures 12 and 13 with the squares.

In Figures 10−13, dispersions are seen for ϵ''_{SIIS} and ϵ''_{SI} at all T. The segmental motion of the S and I blocks has very minor contributions to the ϵ'' data in the ranges of ω and T examined.[8] Thus the dispersions seen in Figures 10−13 are attributed to global relaxation of the I blocks.

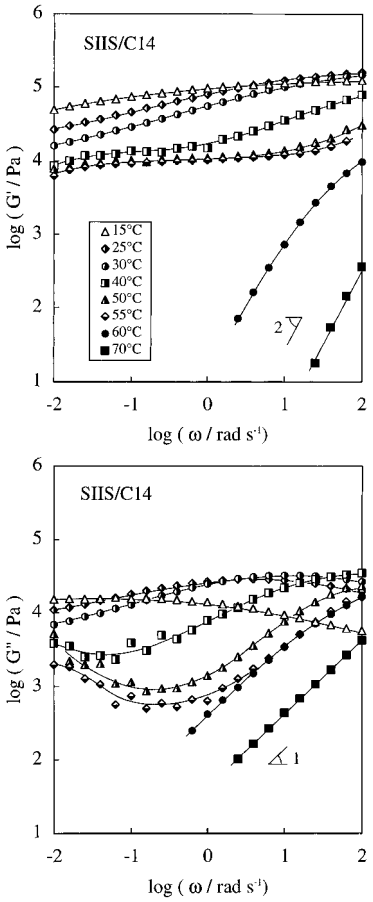

Figure 8. Linear viscoelastic moduli of the SIIS/C_{14} system (c_{SIIS} = 50 wt %) at various temperatures. The unfilled, half-filled, and fully filled symbols indicate that the system is in the rubbery, plastic, and viscous regimes, respectively.

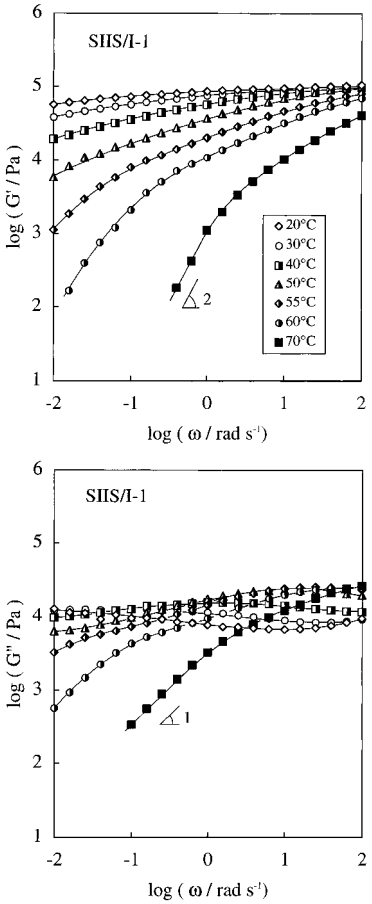

Figure 9. Linear viscoelastic moduli of the SIIS/I-1 system (c_{SIIS} = 45.3 wt %) at various temperatures. The unfilled, half-filled, and fully filled symbols indicate that the system is in the rubbery, plastic, and viscous regimes, respectively.

For the SI chain, the polarization **P** is proportional to the end-to-end vector **R** of its I block (cf. Figure 14) and the dielectric dispersion reflects the fluctuation of **R** due to motion of the I block ends.[17,22] For the SIIS chain having the symmetrical dipole inversion in the I block, **P** is proportional to a difference vector $\Delta\mathbf{R} = \mathbf{R}_1 - \mathbf{R}_2$, with $\mathbf{R}_1$ and $\mathbf{R}_2$ being the two end-to-center vectors depicted in Figure 14. Thus the dispersion of SIIS reflects the fluctuation of $\Delta\mathbf{R}$ due to motion of the ends and the midpoint of the I block.[17] For both cases, the shape (ω dependence) of the ϵ''_{SIIS} and ϵ''_{SI} curves represents the dielectric mode distribution that is determined by the molecular modes of the end/midpoint motion.

At T = 15 °C in C_{14} (Figure 10) and T < 40 °C in I-1 (Figure 12; see the unfilled squares), the SIIS chains exhibit broad dielectric dispersions characterized with a single ϵ''_{SIIS} peak. At respective T, the shape of the ϵ''_{SIIS} curves at the lower-ω side of the peaks is similar to that of the ϵ''_{SI} curves for the SI chains (Figures 11 and 13). Since the S domains are glassy and the motion of the S−I junctions are frozen at those T ($< T_g^{PS}$), these dispersions are exclusively attributable to the midpoint motion of the I blocks for SIIS and to the dangling end motion of the I blocks for SI. (Note that SIS chains without dipole inversion exhibit no dispersion at $T < T_g^{PS}$.)[8]

At those low T (in the rubbery and plastic regimes for SIIS and SI, respectively), terminal relaxation tails ($\epsilon'' \propto \omega$) are not observed at the lower-ω side of the broad ϵ'' peaks and less ω-dependent broad tails are extended down to the lowest ω examined (630 rad s^{-1}). These broad tails, seen more clearly in C_{14} than in I-1 because the peak is located at higher ω in C_{14}, indicate that substantial dielectric modes exist at time scales corresponding to a frequency of 630 rad s^{-1}. Thus the

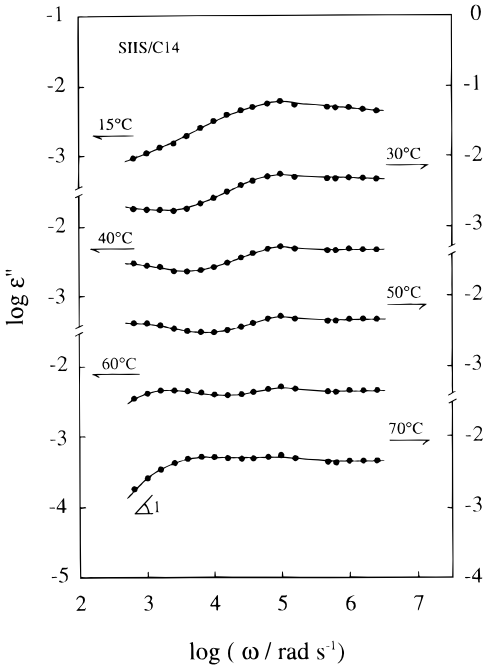

Figure 10. Dielectric loss ϵ'' of the SIIS/C_{14} system (c_{SIIS} = 50 wt %) at various temperatures. The solvent, C_{14}, has no detectable loss at the ω and T examined, and the ϵ'' data represent the dielectric loss ϵ''_{SIIS} of the SIIS chains due to their global motion.

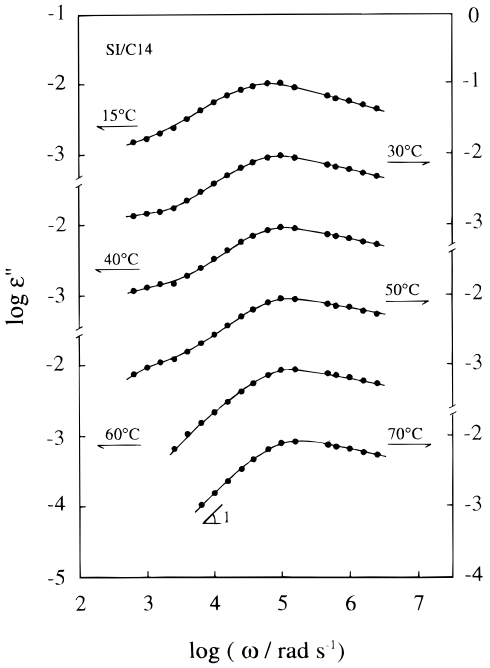

Figure 11. Dielectric loss ϵ'' of the SI/C_{14} system (c_{SI} = 50 wt %) at various temperatures. The solvent, C_{14}, has no detectable loss at the ω and T examined, and the ϵ'' data represent the dielectric loss ϵ''_{SI} of the SI chains due to their global motion.

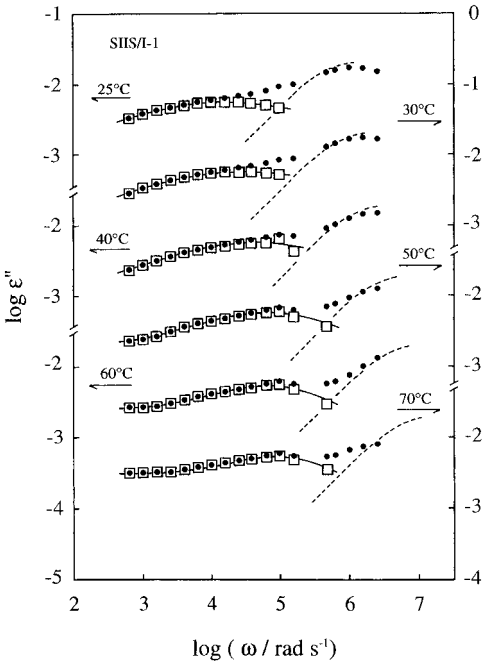

Figure 12. Dielectric loss ϵ'' of the SIIS/I-1 system (c_{SIIS} = 45.3 wt %) at various temperatures (filled circles). The solvent, I-1, has significant contribution to ϵ'' at high ω. The dielectric loss of the SIIS chains, ϵ''_{SIIS} (squares), was evaluated by subtracting the solvent contribution (dotted curves; at respective T, this contribution is common to the SIIS/I-1 and SI/I-1 systems).

terminal dielectric relaxation times τ_ϵ of the SIIS and SI chains are longer than 1.6×10^{-3} s. This τ_ϵ is much larger than τ_ϵ of corresponding homopolyisoprene (hI) chains: For example, $\tau_\epsilon = 2 \times 10^{-6}$ s for a hI/C_{14} solution[23] having the same M (=17.9K) and c (=0.34 g cm^{-3}) as the I block of SI in C_{14}.

All the above results indicate that the SIIS and SI chains exhibit similarly broadened and retarded dielectric relaxation at long time scales in either C_{14} or I-1. However, the ϵ''_{SI} curve is steeper than the ϵ''_{SIIS} curve

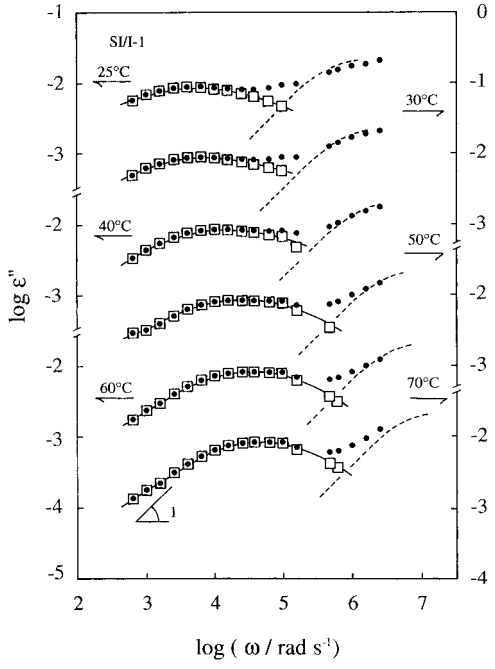

Figure 13. Dielectric loss ϵ'' of the SI/I-1 system (c_{SI} = 45.3 wt %) at various temperatures (filled circles). The solvent, I-1, has significant contribution to ϵ'' at high ω. The dielectric loss of the SI chains, ϵ''_{SI} (squares), was evaluated by subtracting the solvent contribution (dotted curves; at respective T, this contribution is common to the SIIS/I-1 and SI/I-1 systems).

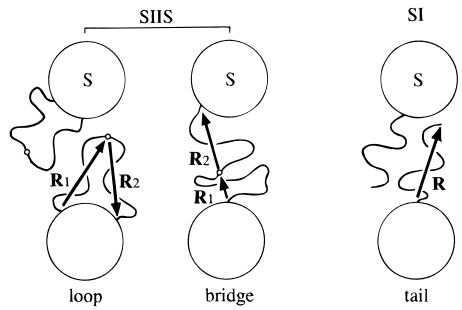

Figure 14. Illustration for the S domains and I blocks for the SIIS and SI systems. The sizes of the S domains and I blocks are shown in proportion to their actual sizes.

at the higher-ω side of their peaks, meaning that the distribution of fast dielectric modes is narrower for the SI chains than for the SIIS chains. We later utilize these similarities and differences to estimate a loop fraction for the I blocks of SIIS.

At intermediate T in the plastic regime for both SIIS and SI (T = 30−50 °C in C_{14} and T = 40−60 °C in I-1; $T > T_g^{PS}$ for both cases), the ϵ''_{SI} and ϵ''_{SIIS} peaks similarly shift to the higher-ω side with increasing T. In addition, an up-turn is seen for the ϵ''_{SI} and ϵ''_{SIIS} curves at low ω, though less prominently in I-1 than in C_{14} because the ϵ'' peak is located at lower ω in I-1. This up-turn suggests that slow dielectric modes emerge at those T.[8]

At higher T in the viscous regime for both SIIS and SI (T = 60 and 70 °C in C_{14} and 70 °C in I-1), the ϵ''_{SI} and ϵ''_{SIIS} curves exhibit different features: For SI in C_{14} (Figure 11), the ϵ''_{SI} peak shifts to higher ω with increasing T, and its low-ω tail becomes steeper to exhibit the terminal behavior ($\epsilon''_{SI} \propto \omega$) at 60 and 70 °C. On the other hand, for SIIS in C_{14} (Figure 10), the ϵ''_{SIIS} peak observed in the rubbery and plastic regimes becomes smeared and the up-turn seen in the plastic regime becomes a low-ω peak with increasing T up to 70 °C. The terminal behavior is attained at the lower-ω

Table 2. Dielectric and Rheological Characteristics of the SIIS/C_{14} and SI/C_{14} Systems in the Viscous Regime

T/°C	$10^4\tau_{chain}$/s	$10^4\tau_G$/s	$10^5 J_e$/Pa^{-1}
		SIIS/C_{14}	
60	18	250	6.2
70	9.4	7.8	1.9
		SI/C_{14}	
60	0.12	13	7.6
70	0.085	(<0.3)[a]	(<1.3)[a]

[a] Upper bound for τ_G and J_e estimated from undetectably small G' (<1 Pa at $\omega = 10^2$ rad s^{-1}).

side of this peak. Qualitatively similar differences are seen for SIIS and SI in I-1 (cf. Figures 12 and 13). However, the terminal relaxation is not observed in I-1 even at 70 °C.

IV. Discussion

We have specified the rubbery, plastic, and viscous regimes for the SIIS/C_{14} and SIIS/I-1 systems. Comparison of dielectric and rheological data of the two systems enables us to obtain some detailed insight for the molecular origins of the rheological behavior. A crucial issue is the different effects of the two solvents, C_{14} and I-1, for conformation/motion of the SIIS chains: I-1 partly screens the osmotic constraint for the I block conformation. In addition, we expect that the S blocks are more soluble in C_{14} than in I-1 and thus they are mixed with the I blocks at lower T in C_{14}.

In the remaining part of this paper, we first compare the viscous responses in C_{14} and I-1 and examine this expectation. Then, we turn our attention to the rubbery and plastic responses of the SIIS chains at lower T. These responses are related with structural features, the domain shape and size as well as the I block conformations (loop/bridge). From this point of view, we specify these features, estimate the loop fraction, and then discuss the contribution of the loop-type I blocks to the equilibrium modulus and yield stress, the latter specifying the elasticity limit, i.e., the onset of vanishingly slow plastic flow. Readers exclusively interested in the elasticity and plasticity of SIIS may skip the next section and directly proceed to section IV-2.

IV.1. Viscous Behavior. For SIIS/SI systems, structural heterogeneity affects differently the viscoelastic and dielectric *terminal* relaxation times τ_G and τ_ϵ.[8] This heterogeneity usually results in broad viscoelastic mode distribution that is sensitively detected as an increase of the steady state recoverable compliance J_e. Considering these points, we here examine whether the S and I blocks are homogeneously mixed or not in the viscous regime.

Behavior in C_{14}. In the viscous regime, the SIIS/C_{14} and SI/C_{14} systems exhibit the linear viscoelastic terminal relaxation tails, $G' \propto \omega^2$ and $G'' \propto \omega$ (Figures 6 and 8). The $\tau_G = [G'/\omega G'']_{\omega\to 0}$ and $J_e = [G'/G''^2]_{\omega\to 0}$ evaluated from these tails are summarized in Table 2. For the SI/C_{14} system at 70 °C, G' was undetectably small (<1 Pa) even at the highest ω examined (10^2 rad s^{-1}). This result gave an estimate, $\tau_G < 3 \times 10^{-5}$ s and $J_e < 1.3 \times 10^{-5}$ Pa^{-1} for the SI/C_{14} system at 70 °C.

For the SI/C_{14} system in the viscous regime ($T \geq 60$ °C), the terminal dielectric relaxation tail ($\epsilon'' \propto \omega$) is observed soon after ω is decreased from the ϵ''_{SI} peak frequency ω_p (cf. Figure 11). This peak corresponds to the terminal dielectric mode, and the relaxation time is evaluated as $\tau_\epsilon = \omega_p^{-1}$.

For the SIIS/C_{14} system at 70 °C, the ϵ''_{SIIS} peak seen at low ω is followed by the terminal tail (cf. Figure 10). At 60 °C, this tail is not detected in our ω-window but the shape of the ϵ''_{SIIS} curve around the low-ω peak is nearly the same as that at 70 °C. Thus, at both 60 and 70 °C, we may assign the low-ω peak to the terminal dielectric mode and evaluate the relaxation time as $\tau_\epsilon = \omega_p^{-1}$.

For the SI chains having no dipole inversion, the terminal dielectric mode corresponds to the slowest eigenmode of global chain relaxation. Thus, the relaxation time of *individual* chains, τ_{chain}, is evaluated as

$$\tau_{chain} = \tau_\epsilon = 1/\omega_p \qquad \text{for SI} \tag{2a}$$

On the other hand, for the SIIS chains with symmetrical dipole inversion in the homogeneous state, the slowest eigenmode is dielectrically inert and the second slowest eigenmode corresponds to the terminal dielectric mode.[16,24] For concentrated hI chains, the characteristic time is longer by a factor of 4 for the slowest eigenmode than for the second slowest eigenmode.[16,24] Utilizing this factor, we can evaluate τ_{chain} of the SIIS chains as

$$\tau_{chain} = 4\tau_\epsilon = 4/\omega_p \qquad \text{for SIIS} \tag{2b}$$

The τ_{chain} values thus obtained are summarized in Table 2.

As seen in Table 2, τ_G is much longer than τ_{chain} for both SIIS/C_{14} and SI/C_{14} systems at 60 °C. This result suggests that the viscoelastic relaxation of the systems is much slower than the relaxation of individual chains and thus related to some sort of structural heterogeneity. This heterogeneity can be further examined from comparison of the J_e data with the compliance $J_e^{(h)}$ in the homogeneous state.

In this state, the viscoelastic mode distribution of the SIIS and SI chains having small S content should to be close to that of homopolyisoprene (hI) chains of the same c (=0.43 g cm^{-3}; 50 wt %) and same M (=50.2K and/or 25.1K). Reduced molecular weights of these hI chains, $M_r = cM/\rho = 23.6$K and 11.8K with ρ being the density of bulk hI, are considerably smaller than a characteristic M_c' (≅60K)[25] for the J_e of bulk hI. In general, the J_e of linear homopolymer chains with $M_r < M_c'$ is close to that of Rouse chains, $J_{e,Rouse} = 2M/5cRT$.[25] (The M-independent J_e, characteristic of well-entangled chains, is observed only for $M_r > M_c'$.)[25] Thus, we can use $J_{e,Rouse}$ as an estimate of $J_e^{(h)}$ at $T = 60-70$ °C,

$$J_e^{(h)} \cong 1.75 \times 10^{-5}\ \text{Pa}^{-1} \qquad \text{for homogeneous SIIS/C}_{14} \tag{3a}$$

$$J_e^{(h)} \cong 0.88 \times 10^{-5}\ \text{Pa}^{-1} \qquad \text{for homogeneous SI/C}_{14} \tag{3b}$$

The J_e data at 60 °C (Table 2) are significantly larger than these $J_e^{(h)}$, confirming that some structural heterogeneity exists at 60 °C to increase J_e. As speculated previously,[8] this structure would be the dynamically heterogeneous, concentration fluctuation patterns[26,27] of the S and I blocks. Corresponding to this structural assignment, the nonlinearity of our SIIS and SI chains seen at 60 °C (Figure 3) might be related with suppression of the fluctuation under large shear.[8,28,29]

For the SIIS chains in C_{14} at 70 °C, τ_G and J_e are close to τ_{chain} and $J_e^{(h)}$, respectively (cf. Table 2 and eq 3a). This result suggests that the linear viscous behavior of those chains at 70 °C corresponds to the relaxation of individual chains and the S and I blocks are almost homogeneously mixed at 70 °C. Similarly, the SI chains (shorter than the SIIS chains) are quite possibly in the

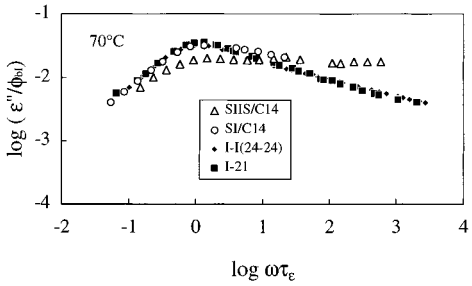

Figure 15. Comparison of ϵ'' data at 70 °C for the SIIS/C_{14} and SI/C_{14} systems with those for bulk hI, I−I 24−24 (M = 48K, with dipole inversion),[24] and I-21 (M = 21K, with no inversion).[24] Those ϵ'' data are reduced by the volume fraction ϕ_{bI} of the I blocks and/or hI chains in the systems and plotted against reduced frequencies $\omega\tau_\epsilon$, with τ_ϵ being the terminal dielectric relaxation time.

homogeneous state in C_{14} at 70 °C, though their τ_G and J_e were too small to be accurately evaluated and the above comparison of τ and/or J_e could not be made on a quantitative basis.

In the rubbery and plastic regimes, the SIIS chains exhibit a broad ϵ''_{SIIS} peak at high ω ($\cong 10^5$ rad s^{-1}; cf. Figure 10). This peak, attributed to the midpoint motion of the I blocks anchored on the S domains, is smeared at 70 °C. This fact also suggests that the S and I blocks are almost homogeneously mixed and the I block ends have a large motional freedom at 70 °C: Such enhanced motion of the I block ends is coupled with the midpoint motion to exhibit a single ϵ''_{SIIS} peak at low ω, as is the case for hI chains having symmetrical dipole inversion.[16,24]

It should be also noted, however, that the shape of the ϵ''_{SIIS} curve (dielectric mode distribution) at 70 °C is not identical to that of hI chains. As shown in Figure 15, the distribution is broader for the SIIS chain (unfilled triangles) than for a dipole-inverted hI chain having nearly the same M (I−I 24−24, M = 48K;[24] filled diamonds). This difference can be partly attributed to the existence of dielectrically inert S blocks for the SIIS chains and also to the concentration fluctuation surviving at 70 °C: This fluctuation appears to be too weak to give detectable effects on J_e and τ_G.

In Figure 15, we also note that the shape of the ϵ'' curve at low ω is roughly the same for the SI chain in C_{14} at 70 °C (unfilled circles) and a corresponding hI chain without dipole-inversion (I-21, M = 21K;[24] filled squares.) Thus, at 70 °C, the fluctuation appears to be much less significant for the SI chains than for the twice longer SIIS chains.

Behavior in I-1. Differing from the behavior in C_{14}, the ϵ''_{SIIS} and ϵ''_{SI} peaks in I-1 are not followed by the terminal relaxation tail (cf. Figures 12 and 13). Those peaks do not correspond to the terminal mode, and τ_{chain} cannot be evaluated from the peak frequencies. Thus we examine the heterogeneity in I-1 through comparison of the J_e data with $J_e^{(h)}$ in the homogeneous state.

$J_e^{(h)}$ for the SIIS and SI chains in I-1 (45.3 wt %) agree, within 10%, with those given in eq 3. The J_e data of the SIIS/I-1 and SI/I-1 systems at 70 °C, 1.1×10^{-4} Pa^{-1} and 1.0×10^{-4} Pa^{-1}, are significantly larger than those $J_e^{(h)}$. Thus, as similar to the situation in C_{14} at 60 °C, the concentration fluctuation would be responsible for the slow, linear viscoelastic relaxation of the SIIS and SI chains in I-1 at 70 °C. Under large shear at 70 °C, the chains in I-1 exhibited nonlinear viscous behavior similar to that seen in Figure 3. This behavior could be due to suppression of the fluctuation under shear.

Here, we note a difference in the structures in C_{14} and I-1 at 70 °C: In C_{14} the SIIS and SI chains are in an almost homogeneous state (with a weak fluctuation), while in I-1 they have a significant dynamic heterogeneity (strong fluctuation). Thus, as anticipated earlier, the S blocks are less soluble and the mixing of the S and I blocks is less easily attained in I-1 than in C_{14}. For the SIIS chains, this difference in the solubilities of C_{14} and I-1 gives a key factor in later discussion for the molecular origin of the plasticity.

IV.2. Domain Structure and I Block Conformation at Low *T*. In the rubbery and plastic regimes at low T, the segregated S blocks form spherical domains in the SIIS and SI systems. Figure 14 depicts those domains together with the I blocks. (Sizes of the S domains and I blocks are shown in proportion to their actual sizes estimated below.) The I blocks of SI are tethered on S domains and have a tail conformation, while the I blocks of SIIS have either a loop or a bridge conformation.

In our concentrated SI solutions (c_{SI} = 50 wt %) containing micellar lattices, a radius of the S domains at low T should be close to that in the bulk state. Thus, we used literature data[30] for bulk systems to estimate the radius in our solutions, $r_S \cong 8$ nm. From this r_S value, the lattice spacing in the solution is evaluated to be ≅33 nm. The average end-to-end distance $\langle \mathbf{R}^2 \rangle^{0.5}$ of the concentrated tail I blocks should be comparable with $2^{0.5} \langle \mathbf{R}^2 \rangle_\theta^{0.5} \cong 16$ nm. Here, $\langle \mathbf{R}^2 \rangle_\theta^{0.5}$ (≅11 nm) is the unperturbed end-to-end distance of the I block (M = 17.9K) evaluated from an empirical equation in the literature,[31] and the factor $2^{0.5}$ accounts for an effect of the S cores that repel the anchored I blocks.[32] These tail (corona) blocks of neighboring micelles are deeply overlapping with each other and subjected to the osmotic constraint.

Bulk A−B−A triblock and A−B/2 type diblock copolymers usually have the same domain size and shape.[33] This should be the case also for the SIIS and its precursor SI chains in our concentrated solutions. Thus we estimate $r_S \cong 8$ nm and $D \cong 33$ nm for our SIIS solutions.

Now we consider conformations of two half-fragments of the middle I block of our SIIS having the end-to-end vectors $\mathbf{R}_1$ and $\mathbf{R}_2$ (cf. Figure 14). Each fragment corresponds to the tail I block of SI. When the middle I block takes the loop conformation, $\mathbf{R}_1$ and $\mathbf{R}_2$ should have an average close to $\langle \mathbf{R}^2 \rangle^{0.5}$ of the tail, $\langle \mathbf{R}_1^2 \rangle^{0.5} = \langle \mathbf{R}_2^2 \rangle^{0.5} \cong 16$ nm. The end-to-end distance of the whole loop, $R = |\mathbf{R}_1 + \mathbf{R}_2|$, is limited to be less than $2r_S$ (≅16 nm). Under this constraint for R, a simple geometrical consideration suggests that repulsion due to impenetrable S domains rules out conformations of the two loop fragments having widely different end-to-end distances R_1 (=$|\mathbf{R}_1|$) and R_2 (=$|\mathbf{R}_2|$). (For these conformations to be realized, a difference $|R_1 - R_2|$ should be comparable with the larger of R_1 and R_2, and the midpoint of the loop should be located near or in the S domain; cf. Figure 14.) In other words, the two loop fragments have $R_1 \cong R_2$ for most of the available conformations.

On the other hand, the S domains provide a much weaker constraint for R_1 and R_2 of the two bridge fragments: For example, R_1 can be much smaller than R_2 if the midpoint of the bridge is located on (or near) a line connecting the bridge ends (cf. Figure 14). (This midpoint location, giving widely different R_1 and R_2, is not allowed for the loop.) Thus, differing from the situation for the loop fragments, many conformations having widely different R_1 and R_2 are available for the

bridge fragments. This difference becomes a key factor for the estimation of the loop fraction explained below.

IV.3. Loop Fraction for SIIS in the Rubbery Regime. Differing from a previously used SIS copolymer,[8] the SIIS copolymer exhibits a significant dielectric dispersion in the rubbery regime due to the dipole inversion in the I block (cf. Figures 10 and 12). As before,[17] we attempt to estimate the loop fraction for those I blocks from the dielectric data of the SIIS and its precursor SI chains.

General Idea. Both loop- and bridge-type I blocks contribute to ϵ'' of the SIIS systems, while only the tail-type I block contributes to ϵ'' of the SI systems. Thus, ϵ'' can be written as[17]

$$\epsilon''_{\mathrm{SIIS}}(\omega) = \int_{-\infty}^{\infty}[\nu_b \Delta\tilde{\epsilon}_b g_b(\tau) + \nu_l \Delta\tilde{\epsilon}_l g_l(\tau)]\frac{\omega\tau}{1+\omega^2\tau^2}\, \mathrm{d}\ln\tau \qquad \text{(for SIIS)} \quad (4a)$$

$$\epsilon''_{\mathrm{SI}}(\omega) = \int_{-\infty}^{\infty}\nu_t \Delta\tilde{\epsilon}_t g_t(\tau)\frac{\omega\tau}{1+\omega^2\tau^2}\, \mathrm{d}\ln\tau \qquad \text{(for SI)} \quad (4b)$$

Here, $\Delta\tilde{\epsilon}_b$, $\Delta\tilde{\epsilon}_l$, and $\Delta\tilde{\epsilon}_t$ are the dielectric intensity per each bridge, loop, and tail I block and ν_b, ν_l, and ν_t are the respective number densities in the system. Note that $\nu_t = 2(\nu_b + \nu_l)$ because the concentration is the same for our SIIS and SI chains (in either C_{14} or I-1) but M_{SIIS} is exactly twice M_{SI}. $g_X(\tau)$ (X = b, l, t) are the dielectric mode distribution functions normalized as

$$\int_{-\infty}^{\infty} g_X(\tau)\, \mathrm{d}\ln\tau = 1 \qquad (X = t, b, l) \quad (5)$$

If we have some information for these mode distribution functions, we can utilize eq 4 to estimate the loop fraction $\phi_l = \nu_l/(\nu_b + \nu_l) = 2\nu_l/\nu_t$ from the ϵ''_{SI} and $\epsilon''_{\mathrm{SIIS}}$ data.

Similarities and Differences of Tail, Loop, and Bridge Motions. In the previous dielectric study[17] for bulk SIIS and SI lamellae aligned essentially parallel to the electrodes, the motion of the loop/bridge-type I blocks of SIIS and tail-type I blocks of SI was detected in a direction essentially perpendicular to the lamellar surfaces. A similarity deduced for the tail and loop motion in this direction and a difference deduced for the loop and bridge motion suggested $g_t(\tau) \cong g_l(\tau) \gg g_b(\tau)$ at large τ, and ϕ_l was estimated from the $\epsilon''_{\mathrm{SIIS}}/\epsilon''_{\mathrm{SI}}$ ratio at low ω. The estimated ϕ_l(≅60%) agreed well with the prediction of the Matsen−Schick theory[34] for triblock copolymer lamellae.

The present SIIS/C_{14} and SI/C_{14} systems contain spherical S domains not aligned with respect to the electrodes, and the ϵ'' data reflect the I block motion averaged over all directions. However, the above similarities and differences can be deduced also for these systems.

To deduce those similarities and differences, we first focus our attention to the broadened and retarded dielectric relaxation of the SI systems at low $T < T_g^{\mathrm{PS}}$ (Figures 11 and 13). This relaxation reflects the dangling end motion of the tail I block, and the broadening and retardation result from a thermodynamic barrier for this motion:[17,22] As explained for Figures 6 and 7, the tail I blocks are osmotically constrained. Thus their large scale motion should take place in a highly cooperative way so as to maintain a uniform distribution of the I block segments. During this cooperative motion, each block has to take an entropically unfavorable, distorted conformation. The resulting entropy loss provides a barrier for the large scale motion of the dangling end, and the dielectric relaxation is retarded and broadened according to the barrier height that is characterized with the end-to-end distance R for the distorted conformation. A similar barrier should exist for the I blocks of SIIS.[17]

At $T < T_g^{\mathrm{PS}}$, the dielectric relaxation of the SIIS system reflects the midpoint motion of the I block. This motion is determined by the entropic barrier as well as by a balance of tension and friction for two half-fragments of the I block. As explained for Figure 14, the end-to-end distances R_1 and R_2 of the two *loop fragments* are nearly the same for most of the available conformations. This suggests that the entropic barriers for the midpoint motion, characterized with R_1 and R_2, are nearly the same for the two fragments and each barrier is similar to that for the tail I block of SI. In addition, the two loop fragments having $R_1 \cong R_2$ exert nearly the same tensile forces to the midpoint, each being close to the tensile force of the tail, and the friction of each fragment is identical to that of the tail. Thus the tension/friction balance would be nearly the same for the loop fragment and tail. These arguments suggests that the two loop fragments together behave as a hypothetical tail to determine the midpoint motion and their dielectric relaxation is retarded and broadened to an extent similar to that for the tail relaxation. (Entanglement effects are not important for our short loop and tail (M = 35.8K and 17.9K) diluted in the C_{14}/I-1 matrices at the concentration $c_{bI} = 0.34$ g cm^{-3}.) This similarity between the loop and tail motion is incorporated in eq 4 through relationships $g_l(\tau) \cong g_t(\tau)$ (nearly the same dielectric mode distribution) and $\Delta\tilde{\epsilon}_l = 2\Delta\tilde{\epsilon}_t$ (twice larger dielectric intensity of a loop containing two fragments each being identical to the tail).

The bridge fragments do not exhibit the above similarity with the tail. As explained for Figure 14, these fragments generally have $R_1 \neq R_2$ to provide different barriers for the midpoint motion. Specifically, a decrease of R_1 for one fragment is canceled by an increase of R_2 for the other fragment when the midpoint moves along a line connecting the bridge ends. Consequently, we expect that an increase of the barrier due to motion of one fragment (characterized with R_1) tends to be canceled, on average, by a decrease of the barrier due to the motion of the other fragment (characterized with R_2). Thus, the net barrier for the midpoint motion appears to be smaller for the bridge than for the loop, suggesting that the dielectric relaxation of the bridge is faster than the loop relaxation. This molecular picture is incorporated in eq 4 through a relationship, $g_b(\tau) \ll g_l(\tau)$ at large τ (less significant slow modes for the bridge). In addition, the two bridge fragments tend to exert tensile forces to the midpoint in the opposite direction. Thus, under the osmotic constraint, the midpoint may be more localized and its motion may have smaller amplitudes for the bridge than for the loop. This argument suggests a relationship $\Delta\tilde{\epsilon}_b < \Delta\tilde{\epsilon}_l$ for eq 4.

The above molecular pictures for the tail, loop, and bridge motion, deduced also for the SIIS and SI lamellae,[17] can be summarized as

$$[\nu_b \Delta\tilde{\epsilon}_b g_b + \nu_l \Delta\tilde{\epsilon}_l g_l(\tau)] \cong \nu_l \Delta\tilde{\epsilon}_l g_l(\tau) \cong 2\nu_l \Delta\tilde{\epsilon}_t g_t(\tau) \qquad \text{at large } \tau \quad (6)$$

From eqs 4 and 6 together with the relationship for the SI and its dimer SIIS chains, $\nu_t = 2(\nu_b + \nu_l)$, we obtain

$$\epsilon''_{\mathrm{SIIS}}(\omega) \cong [\nu_l/(\nu_l + \nu_b)]\epsilon''_{\mathrm{SI}}(\omega) \qquad \text{at low } \omega \quad (7)$$

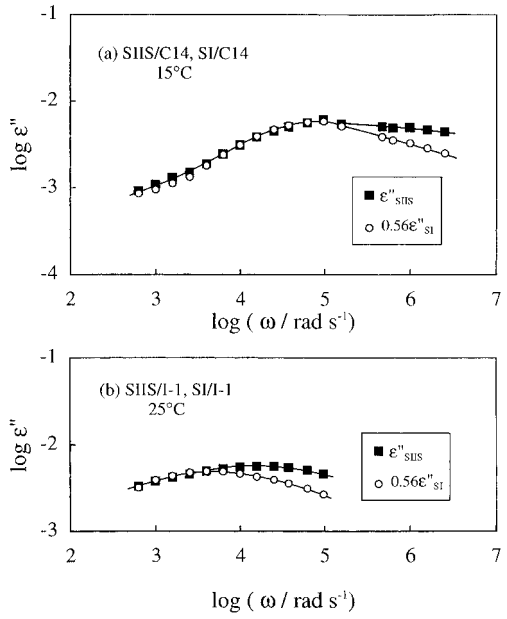

Figure 16. Comparison of $\epsilon''_{SIIS}(\omega)$ and $\epsilon''_{SI}(\omega)$ data in the rubbery regime: (a) for the SIIS and SI chains (50 wt %) in C_{14} at 15 °C; (b) for the SIIS and SI chains (45.3 wt %) in I-1 at 25 °C. The $\epsilon''_{SI}(\omega)$ data are multiplied by a factor 0.56.

From eq 7, we expect that the ω dependence of ϵ'' is the same for the SIIS and SI chains at low ω and the magnitude of ϵ'' is smaller for the former by a factor $\phi_l = \nu_l/(\nu_l + \nu_b)$ (loop fraction). This expectation is examined in Figure 16 where the $\epsilon''_{SIIS}(\omega)$ and $\epsilon''_{SI}(\omega)$ data at low T ($< T_g^{PS}$) are compared for the solutions in C_{14} (part a) and I-1 (part b). According to eq 7, the $\epsilon''_{SI}(\omega)$ curves are multiplied by an appropriate factor ϕ_l to achieve the best superposition on the $\epsilon''_{SIIS}(\omega)$ curves at low ω. In C_{14} (Figure 16a), excellent superposition of the curves is achieved not only at their low-ω tails but also at around the peaks for the factor $\phi_l = 0.56$. This result lends support to eq 7 and the underlying molecular picture, the similarity and difference in the relaxation of tail, loop, and bridge. In I-1, the superposition is achieved also for $\phi_l = 0.56$ (Figure 16b), although the ϵ''_{SIIS} and ϵ''_{SI} data are available only around the peaks and the validity of eq 7 at much lower ω cannot be tested. From these results, we obtain an estimate for the loop and bridge fractions ϕ_l and ϕ_b,

$$\phi_l \cong 60\%, \quad \phi_b \cong 40\%$$
for SIIS in C_{14} and I-1 in the rubbery regime (8)

Comments for the Estimated Loop Fraction. A natural question for eq 8 is whether the estimated ϕ_l includes interdigitated (mutually knotted) loops or not. Under large strain, the interdigitated and dangling (noninterdigitated) loops should exhibit different dynamic responses, the former possibly behaving similarly to the bridges. (This difference is considered in later discussion for the plasticity.) However, in the quiescent state (where the ϵ'' data at $T < T_g^{PS}$ were obtained), a loop would not necessarily realize whether neighboring block chains interdigitate with it or not, unless it moves over large distances at long time scales. Thus, a naive expectation is that all loops are counted in $\phi_l \cong 60\%$ that was not estimated from the ϵ'' data at the *real low-ω limit* where the terminal behavior ($\epsilon'' \propto \omega$) should be observed. This problem of the loop interdigitation deserves further attention.

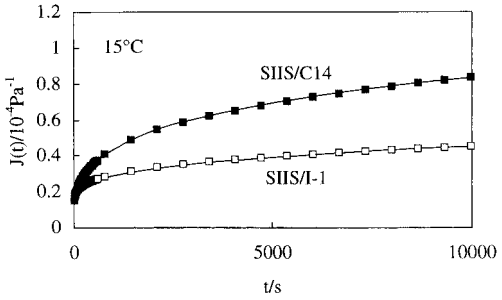

Figure 17. Comparison of linear viscoelastic creep compliance for the SIIS/C_{14} and SIIS/I-1 systems in the rubbery regime (15 °C). The solid curves indicate empirical fitting functions for viscoelastic solids, $J(t) = \sum_p L_p[1 - \exp(-t/\lambda_p)]$ (L_p = discretized retardation spectrum).

It should be also emphasized that a key factor in our estimation of ϕ_l is the osmotic constraint for the I block conformation. To demonstrate this point, we here consider dielectric behavior of osmotically unconstrained loop- and bridge-type Rouse chains of length N and a tail-type Rouse chain of length $N/2$. The bridge and loop chains have symmetrical dipole inversion, and the tail chain has no inversion. We can solve the Rouse equation of motion[35] to calculate ϵ'' for these end-fixed chains if we neglect a spatial constraint for the chains due to impenetrable S domains (having a volume fraction ≅12 vol % in our SIIS and SI systems). As shown in the Appendix, ϵ'' is exactly the same for the three types of chains and for a free (end-unfixed) Rouse chain of length N, meaning that ϕ_l cannot be dielectrically evaluated for the Rouse chains. These features of the Rouse chains are quite different from the features of the SIIS and SI chains, indicating the importance of the thermodynamic effect (osmotic constraint) for motion of actual block chains.

Finally, we emphasize that ϕ_l and ϕ_b for the SIIS systems (eq 8) were estimated on the basis of the molecular picture, the similarity and difference in the tail, loop, and bridge motion. This picture seems to be valid for roughly estimating ϕ_l. However, accurate evaluation of ϕ_l requires a method being based on no molecular picture. Previously explained model systems,[17] blends of SIX, ring SI, and ring XI copolymers (X = a polymeric block immiscible with the S and I blocks) all having symmetrical dipole inversion in the I blocks, serve for this purpose.

IV.4. Origin of Rubbery Behavior of SIIS. An SIS copolymer having no dipole inversion exhibits no dielectric dispersion in the rubbery regime (at $T < T_g^{PS}$).[8] This fact indicates that the rubbery behavior results from a network of *glassy* S domains connected by the I blocks. This molecular picture is further supported from the results of this study: As seen in Figure 5, the rubbery regime is wider for the SIIS/I-1 system than for the SIIS/C_{14} systems, and the boundary between the rubbery and plastic regimes is close to T_g^{PS} in respective systems (≅41 °C in I-1 and ≅30 °C in C_{14}).

The network forming, bridge-type I blocks certainly contribute to the equilibrium moduli G_e^{SIIS} of the SIIS systems. In addition, the loop-type I blocks should also have a contribution when they are osmotically constrained. Utilizing the loop and bridge fractions ϕ_l and ϕ_b estimated in eq 8, we evaluate these contributions below.

Bridge and Loop Contributions to Equilibrium Modulus. For the G' and G'' data of the SIIS/C_{14} and SIIS/I-1 systems in the rubbery regime, weak but slow relaxation processes (characteristic of softly cross-linked

rubbers) are seen at ω as low as 10^{-2} rad s^{-1} (Figures 8 and 9). Since G_e^{SIIS} (=$[G']_{\omega\to 0}$) estimated from those data could contain some uncertainties due to the extrapolation to $\omega = 0$, we evaluated G_e^{SIIS} from creep measurements in the linear viscoelastic regime over time scales significantly longer than that covered in Figures 8 and 9. Figure 17 shows the creep compliance $J(t)$ of the two systems at 15 °C (in the rubbery regime). Although the equilibrium plateau of $J(t)$ is not fully developed for those data at $t \le 10^4$ s, we were able to fit the data with an empirical equation for viscoelastic solids, $J(t) = \sum_p L_p[1 - \exp(-t/\lambda_p)]$ with L_p being a discretized retardation spectrum. This fit, shown with the solid curves in Figure 17, gave

$$G_e^{SIIS} = [1/J(t)]_{t\to\infty} = 0.83 \times 10^4 \text{ Pa for SIIS/C}_{14} \quad (9a)$$

$$G_e^{SIIS} = [1/J(t)]_{t\to\infty} = 1.4 \times 10^4 \text{ Pa for SIIS/I-1} \quad (9b)$$

These G_e^{SIIS} have contributions from the bridge- and loop-type I blocks,

$$G_e^{SIIS} = \nu_b \tilde{G}_e^{(b)} + \nu_{l,i} \tilde{G}_e^{(l,i)} + \nu_{l,d} \tilde{G}_e^{(l,d)} \quad (10)$$

Here, $\tilde{G}_e^{(b)}$ is the equilibrium modulus sustained by each bridge, and $\tilde{G}_e^{(l,i)}$ and $\tilde{G}_e^{(l,d)}$ are the moduli sustained by each interdigitated and dangling loop, respectively. ν_b, $\nu_{l,i}$, $\nu_{l,d}$ (=$\nu_l - \nu_{l,i}$) are the number densities of the bridges and respective loops. (Since the interdigitated and dangling loops might have different moduli, we have separated their contributions in eq 10.)

In our SIIS and SI systems, the I blocks are osmotically constrained and their conformations are distorted under applied strain so as to maintain the uniform distribution of the I block segments in the matrix phase. This fact suggests that the dangling loop-type I blocks exhibit an elastic stress similar to that of the tail (corona) I blocks in the SI micellar systems (before yielding).[36] For concentrated micellar lattice systems, G_e^{SI} is proportional to the tail number density ν_t and the equilibrium modulus sustained by a tail, $\tilde{G}_e^{(t)}$, is independent of the tail molecular weight and concentration.[37] This fact indicates that each tail behaves as an entropic strand. The dangling loop should similarly behave as the entropic strand and its $\tilde{G}_e^{(l,d)}$ should be close to $\tilde{G}_e^{(t)}$. Thus, utilizing the equilibrium modulus G_e^{SI} (=1.4×10^4 Pa in C_{14} and 0.66×10^4 Pa in I-1) and the tail number density ν_t (=9.7×10^{24} m^{-3}) of our SI micellar lattice systems, we may evaluate $\tilde{G}_e^{(1,d)} \cong \tilde{G}_e^{(t)} = G_e^{SI}/\nu_t$ at 15 °C as

$$\tilde{G}_e^{(1,d)} \cong 1.4 \times 10^{-21} \text{ Pa m}^3 \quad \text{for SIIS/C}_{14} \quad (11a)$$

$$\tilde{G}_e^{(1,d)} \cong 0.68 \times 10^{-21} \text{ Pa m}^3 \quad \text{for SIIS/I-1} \quad (11b)$$

(G_e^{SI} of our SI micelles is quite insensitive to T at T ≤ 30 °C (Figures 6 and 7). Thus, we neglected a small difference between 15 °C and 20 °C and used the G_e^{SI} data at 20 °C in the above evaluation.)

The interdigitated loops would also behave as the entropic strands and have $\tilde{G}_e^{(l,i)} \cong \tilde{G}_e^{(t)}$ if they do not realize that they are mutually knotted with each other. On the other hand, those loops would exhibit the elastic behavior similar to that of the bridge if they feel the interdigitation effect. Considering these two possibilities, we may specify a range of $\tilde{G}_e^{(l,i)}$ as

$$\tilde{G}_e^{(l,d)} \le \tilde{G}_e^{(l,i)} \le \tilde{G}_e^{(b)} \quad (12)$$

For both SIIS/C_{14} and SIIS/I-1 systems in the rubbery regime, ν_b and ν_l evaluated from the bridge and loop fractions (eq 8) are

$$\nu_b \cong 1.9 \times 10^{24} \text{ m}^{-3},$$
$$\nu_l = \nu_{l,i} + \nu_{l,d} \cong 2.9 \times 10^{24} \text{ m}^{-3} \quad (13)$$

The number density of the dangling loops, $\nu_{l,d}$, should be in a range,

$$0 \le \nu_{l,d} \le \nu_l \quad (14)$$

From eqs 10−14 and the experimental values for G_e^{SIIS} (eq 9) we can specify a range of $\tilde{G}_e^{(b)}$,

$$1.7 \times 10^{-21} \le \tilde{G}_e^{(b)} \text{ (Pa m}^3\text{)} \le 2.2 \times 10^{-21} \quad \text{for SIIS/C}_{14} \quad (15a)$$

$$2.9 \times 10^{-21} \le \tilde{G}_e^{(b)} \text{ (Pa m}^3\text{)} \le 6.3 \times 10^{-21} \quad \text{for SIIS/I-1} \quad (15b)$$

It should be noted that the $\tilde{G}_e^{(b)}$ value for the SIIS/C_{14} system (eq 15a) is specified within a small uncertainty (±15%) despite rather wide ranges allowed for $\tilde{G}_e^{(l,i)}$ (eq 12) and $\nu_{l,d}$ (eq 14).

Comparison of eqs 11a and 15a indicates that a difference between $\tilde{G}_e^{(l,d)}$ and $\tilde{G}_e^{(b)}$ for the SIIS/C_{14} system is surprisingly small (less than a factor of 1.6). Correspondingly, the elasticity of this system has almost equal contributions from the bridges and loops: The ratio of these contributions is $\nu_b\tilde{G}_e^{(b)}/[\nu_{l,i}\tilde{G}_e^{(l,i)} + \nu_{l,d}\tilde{G}_e^{(l,d)}]$ = 0.63−1.0 (cf., eqs 9a, 13, and 15a). These results suggest that the osmotic constraint for the loops strongly contributes to the elasticity of our SIIS/C_{14} system in the rubbery regime. On the other hand, for the SIIS/I-1 system (eqs 11b and 15b), $\tilde{G}_e^{(l,d)}$ is considerably smaller than $\tilde{G}_e^{(b)}$ because of the partial screening of the osmotic constraint in the I-1 matrix. The elasticity in this matrix appears to be dominated by the bridges (and interdigitated loops).

Comments for the Bridge Contribution to G_e. The reduced molecular weight of the I blocks of SIIS in the C_{14} matrix, $M_r = c_{bI}M/\rho \cong 13$K with c_{bI} and ρ being the I block concentration in the matrix and bulk hI density, is only slightly larger than the characteristic M_c (=10K)[25] for viscosity of bulk hI. Those I blocks would hardly form trapped entanglements. Thus each bridge (and interdigitated loop) should essentially behave as an entropic strand *as a whole*, as is the case also for the osmotically constrained dangling loop. This naturally explains the close agreement of $\tilde{G}_e^{(b)}$ and $\tilde{G}_e^{(l,d)}$ (eqs 11a and 15a).[38]

The other point to be noted is the difference of $\tilde{G}_e^{(b)}$ in C_{14} and I-1 (eqs 15a and 15b). $\tilde{G}_e^{(b)}$ appears to be larger in I-1 than in C_{14}, although the large uncertainty for $\tilde{G}_e^{(b)}$ in I-1 does not allow us to accurately evaluate the difference. This result might mean that the elasticity of the bridges is enhanced when the osmotic constraint is screened. A further study is necessary for this difference.

IV.5. Origin of Plastic Behavior of SIIS. Assignment of Up-Turn and Peak in ϵ''. In the plastic regime ($T > T_g^{PS}$), the SIIS and SI chains exhibit the

up-turn in their ϵ'' curves at low ω (Figures 10−13). The S blocks are in the liquid state and the S-I junctions have some motional freedom in this regime. As discussed previously,[8] the up-turn is attributable to the junction motion in the S/I interfaces.[39]

For SIIS, this junction motion should be more restricted and slower than the motion of the midpoint of the I blocks. Thus the ϵ''_{SIIS} peak in the plastic regime, seen at higher ω than the up-turn (Figures 10 and 12), is attributable to the midpoint motion. Similarly, the ϵ''_{SI} peak for the SI systems in the plastic regime (Figures 11 and 13) is attributed to the dangling end motion of the I blocks.

Loop Fraction in the Plastic Regime. In the plastic regime, the motion of the S−I junctions is not necessarily similar for the SIIS and SI chains. Thus, a similarity in the ϵ''_{SIIS} and ϵ''_{SI} data vanishes at low ω where this motion is detected as the up-turn of ϵ'', and the loop fraction ϕ_l cannot be estimated from the data at those ω. However, at higher ω where the ϵ''_{SIIS} peak attributable to the midpoint motion is observed, the junction motion would be practically frozen and ϕ_l may be estimated on the basis of the molecular picture deduced for the end-fixed I blocks.

In the rubbery regime, the ϵ''_{SIIS} and ϵ''_{SI} curves exhibit excellent superposition in their low-ω tails as well as around their peaks (cf. Figure 16). This result, suggesting a minor contribution of the bridges to the ϵ''_{SIIS} peaks, enables us to extend the ω-range usable for estimation of ϕ_l up to the ϵ''_{SIIS} peak frequency. The bridges would have minor contributions to the ϵ''_{SIIS} peak also in the plastic regime, and the $\epsilon''_{SIIS}(\omega)$ and $\epsilon''_{SI}(\omega)$ curves are expected to be superposable around their peaks to give $\phi_l = \epsilon''_{SIIS}(\omega)/\epsilon''_{SI}(\omega)$ (cf. eq 7). In fact, good superposition was achieved in a ω-range covering 1−1.5 decades around the ϵ''_{SIIS} peak frequency (cf. Figures 10−13), and we estimated ϕ_l in the plastic regime from the $\epsilon''_{SIIS}(\omega)$ and $\epsilon''_{SI}(\omega)$ data at those ω.

The ϕ_l values thus obtained were insensitive to T and close to those in the rubbery regime (eq 8). This T-insensitivity is in harmony with the prediction of the Matsen−Schick theory[34] at T not very close to T_{ODT}, though the theory is formulated for lamellar domains, not for the spherical domains involved in our systems.

The above estimate for ϕ_l in the plastic regime is a very rough estimate because the underlying molecular picture is deduced for the end-fixed I blocks. However, this rough estimate still allows us to conclude that the loop and bridge populations are roughly the same in the plastic regime.

For the SIIS/C_{14} and SIIS/I-1 systems in the plastic regime as well as for a previously examined SIS/C_{14} system,[8] flow does not induce detectable dielectric changes. On the basis of the above conclusion, this flow insensitivity is related to the heterogeneity in the flow profile and the population of the bridges. The flow is concentrated in the grain boundary regions that contain only a small population of the SIIS chains, and the number of the bridges (and interdigitated loops) pulling out the S blocks under flow is even smaller because of the coexisting dangling loops. Thus the resulting dielectric changes seem to be too small to be detected.[40]

Loop and Bridge Contributions To Yield Stress. The yield stress σ_y is contributed from the loops and bridges (having roughly the same populations in the plastic regime),

$$\sigma_y = \nu_b \tilde{\sigma}_y^{(b)} + \nu_{l,i} \tilde{\sigma}_y^{(l,i)} + \nu_{l,d} \tilde{\sigma}_y^{(l,d)} \qquad (16)$$

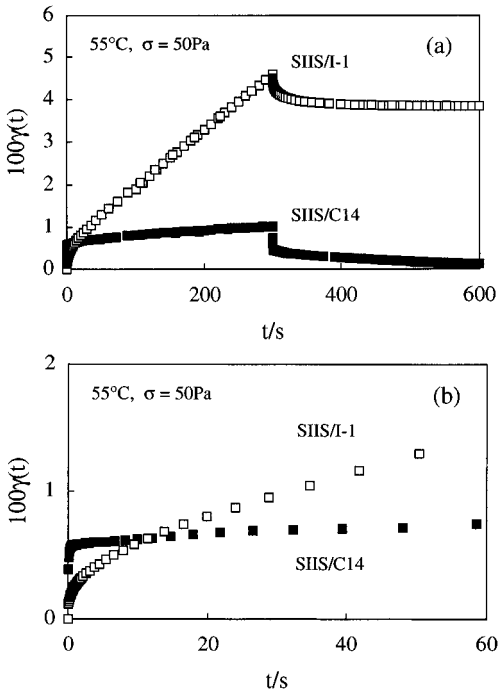

Figure 18. Changes in the strain $\gamma(t)$ with time during creep and recovery measurements for the SIIS/C_{14} and SIIS/I-1 systems at 55 °C. A stress, $\sigma = 50$ Pa, is imposed at $t = 0-300$ s and released at $t > 300$ s. Part b magnifies the changes at short time scales.

Here, $\tilde{\sigma}_y^{(b)}$ is the yield stress sustained by each bridge, and $\tilde{\sigma}_y^{(l,i)}$ and $\tilde{\sigma}_y^{(l,d)}$ are the yield stresses sustained by each interdigitated and dangling loop, respectively. $\tilde{\sigma}_y^{(b)}$, $\tilde{\sigma}_y^{(l,i)}$, and $\tilde{\sigma}_y^{(l,d)}$ should change with the solvent nature in the following way.

The plasticity of the bridges emerges when they pull out the S blocks from S domains, and the corresponding $\tilde{\sigma}_y^{(b)}$ is determined by an enthalpic barrier for mixing of the S and I blocks. As noted in the viscous regime, the mixing is less easily attained in I-1 than in C_{14} and this barrier is larger in I-1. This fact indicates that $\tilde{\sigma}_y^{(b)}$ is larger in I-1 than in C_{14}. Under large strain, the interdigitated loops should also pull out the S blocks and their $\tilde{\sigma}_y^{(l,i)}$ would be similar in nature to $\tilde{\sigma}_y^{(b)}$ of the bridges. Thus, $\tilde{\sigma}_y^{(l,i)}$ should be larger in I-1 than in C_{14}.

On the other hand, the dangling loops exhibit the plasticity due to the osmotic constraint for their conformation, as is the case also for the tail (corona) I blocks of the SI micelles. This constraint is (partly) screened when the solvent is switched from C_{14} to I-1, as confirmed for those micelles (cf. Figures 6 and 7). Consequently, $\tilde{\sigma}_y^{(l,d)}$ should be smaller in I-1 than in C_{14}. (In fact, the decrease of σ_y due to screening of the osmotic constraint has been found for diblock copolymer micelles.[14,15,37])

Considering the above difference of $\tilde{\sigma}_y^{(b)}$, $\tilde{\sigma}_y^{(l,i)}$, and $\tilde{\sigma}_y^{(l,d)}$, we can compare σ_y of the SIIS/C_{14} and SIIS/I-1 systems to examine whether the plasticity is dominated by the dangling loops: These loops dominate the plasticity of the SIIS/C_{14} system if σ_y is larger for this system, and *vice versa*.

Figure 18 demonstrates changes in the strain $\gamma(t) = \sigma J(t)$ with time during creep and recovery measurements for the SIIS/C_{14} and SIIS/I-1 systems at 55 °C, the high-T side in respective plastic regimes. A constant stress, $\sigma = 50$ Pa, is imposed at $t = 0-300$ s and released at $t > 300$ s. Clearly, the SIIS/C_{14} system behaves as a soft solid: It deforms immediately on imposition of this

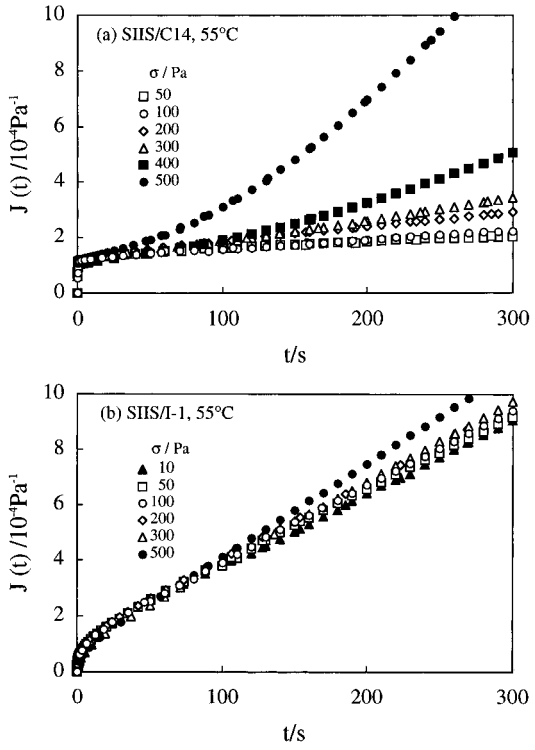

Figure 19. Comparison of (nonlinear) creep compliance at 55 °C for (a) SIIS/C_{14} and (b) SIIS/I-1 systems.

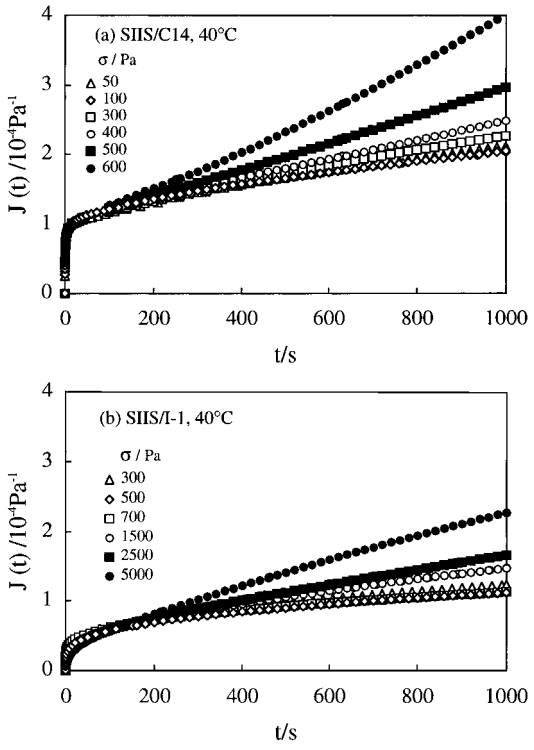

Figure 20. Comparison of (nonlinear) creep compliance at 40 °C for (a) SIIS/C_{14} and (b) SIIS/I-1 systems.

small stress, exhibits retarded deformation of small magnitudes, and fully recovers the strain after release of the stress. On the other hand, the SIIS/C_{14} system flows at constant rate ($t = 150-300$ s) and exhibits only partial recovery of the strain ($t > 300$ s), though it exhibits stronger retardation and has smaller $\gamma(t)$ than the SIIS/C_{14} system at short time scales (cf. Figure 18b). Thus, for $\sigma = 50$ Pa, the SIIS/I-1 system shows liquidlike behavior at long time scales. These results indicate that the SIIS chains have $\sigma_y > 50$ Pa in C_{14} and $\sigma_y < 50$ Pa in I-1.

σ_y can be quantitatively evaluated in Figure 19 where the creep compliance $J(t)$ obtained for various σ is shown for the SIIS/C_{14} and SIIS/I-1 systems at 55 °C. For $\sigma \leq 100$ Pa, $J(t)$ of the SIIS/C_{14} system is independent of σ, and linear viscoelastic, solidlike behavior prevails (Figure 19a). For $\sigma \geq 200$ Pa, this system exhibits σ-dependent (nonlinear) $J(t)$ and behaves as a plastic fluid. Thus σ_y of the SIIS/C_{14} systems is evaluated to be 150 $\pm$ 50 Pa. On the other hand, Figure 19b demonstrates that the SIIS/I-1 system exhibits flow even for $\sigma = 10$ Pa and thus has $\sigma_y < 10$ Pa. These results clearly indicate that σ_y of the SIIS chains is much smaller in I-1 than in C_{14}. Thus, we conclude that the plasticity of the SIIS/C_{14} system at 55 °C is dominated by the dangling loops.

Here, it should be emphasized that the dominant contribution of the dangling loops to σ_y is concluded at 55 °C, the high T side in the plastic regime. At this T, the enthalpic barrier for mixing of the S and I blocks is rather small, and the contribution of the bridges and interdigitated loops is overwhelmed by the contribution of the dangling loops in C_{14}. With decreasing T, this barrier is increased to enhance the former contribution, and this enhancement should be stronger in I-1 than in C_{14}. (I-1 is a poorer solvent for the S blocks.) Thus, we expect that the bridges and interdigitated loops significantly contribute to σ_y at low T, in particular in I-1. We can confirm this expectation at 40 °C (just above the boundary between the rubbery and plastic regimes for the SIIS/I-1 system): As noted from the $J(t)$ data shown in Figure 20, the SIIS/C_{14} system has $\sigma_y \cong 300$ Pa while the SIIS/I-1 system has $\sigma_y = 1100 \pm 400$ Pa at 40 °C. For both systems, σ_y is increased with decreasing T from 55 to 40 °C. However, this increase is much larger in I-1 (from $\sigma_y < 10$ Pa to $\sigma_y \cong 1100$ Pa) than in C_{14} (from $\sigma_y \cong 150$ Pa to $\sigma_y \cong 300$ Pa).

The above result strongly suggests that σ_y of the SIIS/I-1 system at 40 °C is dominated by the bridges and interdigitated loops. The situation is different for the SIIS/C_{14} system at 40 °C: The osmotically determined $\tilde{\sigma}_y^{(l,d)}$ of the dangling loops would be insensitive to a rather small change in T from 55 to 40 °C. Thus, the contribution of these loops to σ_y at 40 °C should be close to that at 55 °C, $\cong$150 Pa (cf. Figure 19). Subtracting this contribution from σ_y of the system at 40 °C ($\cong$300 Pa), the yield stress due to the bridges and interdigitated loops is evaluated to be $\cong$150 Pa. Thus, at 40 °C, σ_y of the SIIS/C_{14} system appears to be *almost equally* contributed from the dangling loops and bridges/interdigitated loops.[41]

V. Concluding Remarks

We have compared rheological and dielectric responses of the dipole-inverted SIIS chains in I-selective solvents, C_{14} and I-1, to examine the molecular origins of their rubbery, plastic, and viscous behavior at low, intermediate, and high T. Comparison of dielectric and viscoelastic relaxation times and examination of the steady state recoverable compliance strongly suggest that the S and I blocks are more or less homogeneously mixed in the viscous regime: The linear viscous behavior seen at the high T part of this regime is attributed to relaxation of individual SIIS chains in a statically homogeneous state, and the nonlinear viscous behavior at the low T part, to relaxation of dynamically heterogeneous structures (concentration fluctuation patterns near T_{ODT}).

In the rubbery and plastic regimes at low T, the I blocks of the SIIS chains take either the loop or bridge

conformations having their ends on the segregated S domains. In both regimes, the loop fraction is dielectrically estimated to be ≅60% in C_{14} and I-1. A crucial factor for the rubbery and plastic responses of the SIIS chains is the osmotic constraint for those loops that is weaker in I-1 than in C_{14}. Comparison of the rheological and dielectric behavior of the SIIS and SI chains in I-1 and C_{14} enables us to examine the loop and bridge contributions to the elasticity and plasticity of the SIIS systems.

The rubbery behavior at $T < T_g^{PS}$ results from a network structure of the glassy S domains connected by the bridge-type I blocks. Nevertheless, for our SIIS systems having relatively short (barely entangled) I blocks, the equilibrium modulus in C_{14} has almost equal contributions from the loops and bridges. This large contribution of the loops reflects the distortion of the loops under strain due to the strong osmotic constraint in C_{14}. This contribution becomes less significant in the polymeric solvent, I-1, which (partly) screens the osmotic constraint.

An importance of the dangling loops is found also for the plasticity of the SIIS chains. At high T where the S/I mixing barrier is rather small, these loops dominate the yield stress. This result is again attributed to the distortion of the loops under strain due to the strong osmotic constraint in C_{14}. On the other hand, the bridges and interdigitated loops exhibit significant yield stresses (due to S/I mixing on pull-out of the S blocks) under an enhanced mixing barrier, i.e., when T is decreased and/or the solvent is switched from C_{14} to I-1, a poorer solvent for the S blocks.

Acknowledgment. We acknowledge with thanks the financial support for this study from the Ministry of Education, Science, Sports, and Culture, Japan, under Grant No. 08875194.

Appendix. ϵ'' for Bridge-, Loop-, and Tail-Type Rouse Chains

We consider a Rouse chain at equilibrium. The chain is composed of $N + 1$ segments (beads), each having a friction ζ, and the nth segment is located at $\mathbf{r}(n,t)$ at time t. If the chain has a fixed end-to-end vector $\mathbf{R}_e$ ($\mathbf{r}(0,t) = \mathbf{0}$ and $\mathbf{r}(N,t) = \mathbf{R}_e$), $\mathbf{r}(n,t)$ can be expanded with respect to sinusoidal eigenfunctions having amplitudes $\mathbf{X}_p$,

$$\mathbf{r}(n,t) = \sum_{p\geq 1} \mathbf{X}_p(t) \sin\left(\frac{p\pi n}{N}\right) + \left(\frac{n\mathbf{R}_e}{N}\right) \qquad \text{(A1)}$$

In a continuous limit (for $N \gg 1$), a time evolution of $\mathbf{X}_p$ calculated from the Rouse equation of motion[35] is

$$\mathbf{X}_p(t) = \mathbf{X}_p(0) \exp[-t/\tau_p] + \frac{2}{N}\int_0^t \mathrm{d}t' \exp[-(t-t')/\tau_p] \times \int_0^N \mathrm{d}n\, \mathbf{f}_B(n,t') \sin\left(\frac{p\pi n}{N}\right) \qquad \text{(A2)}$$

with

$$\tau_p = \frac{\zeta a^2 N^2}{3\pi^2 p^2 kT} \qquad \text{(A3)}$$

Here, a^2 is a mean-square end-to-end distance of a bond vector $\mathbf{u}(n,t) = \partial\mathbf{r}(n,t)/\partial n$ (continuous limit expression), and $\mathbf{f}_B(n,t')$ is the Brownian force acting on the nth segment at time t'.

For chains having parallel dipoles, fundamental features of dielectric relaxation are described by a local correlation function, $C(n,t;m) = (1/a^2)\langle \mathbf{u}(n,t)\cdot\mathbf{u}(m,0)\rangle$.[24] (Here, $\langle ... \rangle$ denotes an equilibrium average.) From eq A2, this function is written as

$$C(n,t;m) = \frac{1}{a^2}\sum_{p\geq 1}\left(\frac{p\pi}{N}\right)^2 \langle \mathbf{X}_p{}^2\rangle \cos\left(\frac{p\pi n}{N}\right) \times \cos\left(\frac{p\pi m}{N}\right) \exp(-t/\tau_p) + \left(\frac{\mathbf{R}_e}{Na}\right)^2 \qquad \text{(A4)}$$

(In deriving eq A4, we used relationships[35] $\langle \mathbf{f}_B(n,t')\rangle = \mathbf{0}$, $\langle \mathbf{f}_B(n,t')\cdot\mathbf{X}_q(0)\rangle = 0$, $\langle \mathbf{X}_p(0)\rangle = \mathbf{0}$, and $\langle \mathbf{X}_p(0)\cdot\mathbf{X}_q(0)\rangle = \delta_{pq}\langle \mathbf{X}_p{}^2\rangle$.) From a Gaussian distribution function for $\mathbf{X}_p$,[35] $\langle \mathbf{X}_p{}^2\rangle$ is calculated to be $2Na^2/p^2\pi^2$. Substituting this result in eq A4, we obtain,

$$C(n,t;m) = \frac{2}{N}\sum_{p\geq 1}\cos\left(\frac{p\pi n}{N}\right) \cos\left(\frac{p\pi m}{N}\right) \times \exp(-t/\tau_p) + \left(\frac{\mathbf{R}_e}{Na}\right)^2 \qquad \text{(A5)}$$

For the chain having dipole inversion at the n^*th segment, a normalized dielectric relaxation function is calculated from $C(n,t;m)$,[24]

$$\Phi_\epsilon(t) = \frac{1}{N}\left[\int_0^{n^*}\mathrm{d}n - \int_{n^*}^{N}\mathrm{d}n\right]\left[\int_0^{n^*}\mathrm{d}m - \int_{n^*}^{N}\mathrm{d}m\right] C(n,t;m) \qquad \text{(A6)}$$

The dielectric loss ϵ'' is a Fourier transformation of $\mathrm{d}\Phi_\epsilon(t)/\mathrm{d}t$ with respect to t,

$$\epsilon''(\omega) = -\Delta\epsilon\int_0^\infty \frac{\mathrm{d}\Phi_\epsilon(t)}{\mathrm{d}t}\sin\omega t\, \mathrm{d}t \qquad \text{(A7)}$$

where $\Delta\epsilon$ is the dielectric relaxation intensity. The fixed end-to-end vector $\mathbf{R}_e$ is not involved in the derivative, $\mathrm{d}\Phi_\epsilon(t)/\mathrm{d}t$. Thus, $\epsilon''(\omega)$ of the Rouse chain does not depend on $\mathbf{R}_e$, meaning that $\epsilon''(\omega)$ is the same for loop- and bridge-type Rouse chains.

For the end-fixed Rouse chains having symmetrical dipole inversion ($n^* = N/2$), eqs A5−A7 give

$$\epsilon''(\omega) = \Delta\epsilon\sum_{p=\mathrm{odd}}\frac{8}{p^2\pi^2}\frac{\omega\tau_p}{1+\omega^2\tau_p{}^2} \qquad \text{(A8)}$$

This $\epsilon''(\omega)$ is identical to $\epsilon''(\omega)$ of a free (end-unfixed) Rouse chain[24] that is composed of N segments and has no dipole inversion.

Now, we consider a tail-type Rouse chain composed of $N/2$ segments (=a half fragment of the loop and bridge chains examined above). Considering the boundary condition for the tail chain, $\mathbf{r}(0,t) = \mathbf{0}$ (for the fixed end) and $[\partial\mathbf{r}(n,t)/\partial n]_{n=N/2} = \mathbf{0}$ (for the free end), we can expand $\mathbf{r}(n,t)$ of this chain with respect to odd, sinusoidal eigenfunctions,

$$\mathbf{r}(n,t) = \sum_{p=\mathrm{odd}}\mathbf{Y}_p(t)\sin\left(\frac{p\pi n}{N}\right) \qquad \text{(A9)}$$

From the time evolution of the amplitude $\mathbf{Y}_p$ obtained from the Rouse equation of motion, the local correlation function for the tail chain is calculated to be

$$C(n,t;m) = \frac{2}{N}\sum_{p=\mathrm{odd}}\cos\left(\frac{p\pi n}{N}\right)\cos\left(\frac{p\pi m}{N}\right)\exp(-t/\tau_p) \qquad \text{(A10)}$$

For the tail chain having no dipole inversion, $\Phi_\epsilon(t)$ is obtained by integrating $C(n,t;m)$ with respect to n and m in a range, $0 < n, m < N/2$, and ϵ'' is calculated from eq A7. The resulting ϵ'' is identical to ϵ'' for the dipole-inverted loop and bridge chains composed of N segments (eq A8).

References and Notes

(1) Holden, G.; Bishop, E. T.; Legge, N. R. *J. Polym. Sci.* **1969**, *C26*, 37.
(2) Chung, C. I.; Gale, J. C. *J. Polym. Sci., Polym. Phys. Ed.* **1976**, *14*, 1149.
(3) Chung, C. I.; Lin, M. I. *J. Polym. Sci., Polym. Phys. Ed.* **1978**, *16*, 545.
(4) Chung, C. I.; Griesbach, H. L.; Young, L. *J. Polym. Sci., Polym. Phys. Ed.* **1980**, *18*, 1237.
(5) Gouinlock, E. V.; Porter, R. S. *Polym. Eng. Sci.* **1977**, *17*, 535.
(6) Pico, E. R.; Williams, M. C. *Polym. Eng. Sci.* **1977**, *17*, 573.
(7) Watanabe, H.; Kuwahara, S.; Kotaka, T. *J. Rheol.* **1984**, *28*, 393.
(8) Sato, T.; Watanabe, H.; Osaki, K. *Macromolecules* **1996**, *29*, 6231.
(9) Winey, K. I.; Patel, S. S.; Larson, R. G.; Watanabe, H. *Macromolecules* **1993**, *26*, 2542, 4373.
(10) Koppi, K. A.; Tirrell, M.; Bates, F. S.; Almdal, K.; Colby, R. H. *J. Phys. II (Fr.)* **1992**, *2*, 1941.
(11) (a) Morrison, F. A.; Winter, H. *Macromolecules* **1989**, *22*, 3533. (b) Morrison, F. A.; Winter, H.; Gronski, W.; Barnes, J. D. *Macromolecules* **1990**, *23*, 4200.
(12) (a) Balsara, N. P.; Garetz, B. A.; Dai, H. J. *Macromolecules* **1992**, *25*, 6072. (b) Balsara, N. P.; Dai, H. J.; Watanabe, H.; Sato, T.; Osaki, K. *Macromolecules* **1996**, *29*, 3507.
(13) Watanabe, H.; Kotaka, T.; Hashimoto, T.; Shibayama, M.; Kawai, H. *J. Rheol.* **1982**, *26*, 153.
(14) Watanabe, H.; Kotaka, T. *J. Rheol.* **1983**, *27*, 223.
(15) Watanabe, H.; Kotaka, T. *Polym. Eng. Rev.* **1984**, *4*, 73.
(16) Yoshida, H.; Watanabe, H.; Adachi, K.; Kotaka, T. *Macromolecules* **1991**, *24*, 2981.
(17) Watanabe, H. *Macromolecules* **1995**, *28*, 5006.
(18) See, for example: Molau, G. E. In *Block Copolymers*; Aggarwal, S. L., Ed.; Plenum Press: New York, 1970.
(19) Watanabe, H.; Kotaka, T. *Polym. J.* **1982**, *14*, 739.
(20) Watanabe, H.; Kotaka, T. *Polym. J.* **1983**, *15*, 337.
(21) The micelles are highly concentrated ($c_{SI} = 45.3$ wt %) in our SI/I-1 system, and the I-1 chains can only partly screen the osmotic constraint. Thus the micellar lattice survives in this system at low T, though its stability is reduced. For less concentrated micelles,[14,15] the matrix chains completely screen the constraint to induce lattice disordering: Those micelles exhibit the viscous (or viscoelastic) behavior with $G_e = 0$.[14,15]
(22) Yao, M. L.; Watanabe, H.; Adachi, K.; Kotaka, T. *Macromolecules* **1991**, *24*, 6175,
(23) This τ_ϵ value, 2×10^{-6} s, was evaluated by extrapolating the τ_ϵ data for hI/C_{14} solutions[22] of various M and c.
(24) Watanabe, H.; Urakawa, O.; Kotaka, T. *Macromolecules* **1993**, *26*, 5073; **1994**, *27*, 3525. Watanabe, H.; Yamada, H.; Urakawa, O. *Macromolecules* **1995**, *28*, 6443.
(25) See for example: Ferry, J. D. *Viscoelastic Properties of Polymers*, 3rd ed.; Wiley: New York, 1980.
(26) Fredrickson, G. H.; Helfand, E. *J. Chem. Phys.* **1987**, *87*, 697.
(27) (a) Rosedale, J. H.; Bates, F. S. *Macromolecules* **1990**, *23*, 2329. (b) Bates, F. S.; Rosedale, J. H.; Fredrickson, G. H. *J. Chem. Phys.* **1990**, *92*, 6255.
(28) Koppi, K. A.; Tirrell, M.; Bates, F. S. *Phys. Rev. Lett.* **1993**, *70*, 1449.
(29) Balsara, N. P.; Hammouda, B.; Kesani, P. K.; Jonnalagadda, S. V.; Straty, G. C. *Macromolecules* **1994**, *27*, 2566.
(30) This r_S value, $\cong$8 nm, was estimated from Figure 12 of ref 33a where literature data for r_S are accumulated for bulk SI, SB, and SBS systems containing spherical S domains.
(31) (a) R_g (radius of gyration) $= 3.35 \times 10^{-2}\ M^{0.5}$ nm for PI chains in a theta solvent.[31b] (b) Tsunashima, Y.; Hirata, M.; Nemoto, N.; Kurata, M. *Macromolecules* **1988**, *21*, 1107.
(32) (a) This factor, $2^{0.5}$, was evaluated for ideal chains grafted on an impenetrable, flat wall.[32b] (b) Dimarzio, E. A. *J. Chem. Phys.* **1965**, *42*, 2101.
(33) (a) Hashimoto, T.; Fujimura, M.; Kawai, H. *Macromolecules* **1980**, *13*, 1660. (b) Hashimoto, T. In *Polymer Alloy*, 1st ed.; Kotaka, T., Ide, F., Ogino, K., Nishi, T., Eds.; Tokyo Kagaku Dojin: Tokyo, 1981.
(34) Matsen, M. W.; Schick, M. *Macromolecules* **1994**, *27*, 187.
(35) See, for example: Doi, M.; Edwards, S. F. *The Theory of Polymer Dynamics*; Clarendon: Oxford, U.K., 1986.
(36) The similarity in the elastic stresses of the loops and tails may vanish if the loops are dilute and embedded in a matrix of bridges. However, in our SIIS systems having highly populated loops ($\phi_l > \phi_b$), the similarity should be valid. Thus we estimate the loop and bridge contribution to equilibrium moduli on the basis of this similarity.
(37) (a) Watanabe, H. *J. Soc. Rheol. Jpn.* **1994**, *22*, 193. (b) Watanabe, H. In *Structures and Properties of Multi-phase Polymeric Materials*; Araki, T., Ed.; Marcel Dekker: New York (in press). (c) Watanabe, H. *Acta Polym.*, in press.
(38) If M_r of the I blocks is significantly larger than M_c, they can form trapped entanglements by taking the bridge/interdigitated loop conformations. For this case, each I block behaves as an ensemble of M/M_e entropic strands (M_e = entanglement spacing). On the other hand, the dangling loop behaves as an entropic strand as a whole irrespective of its M (similar to the behavior of the tail having c- and M-independent $\tilde{G}_e^{(t)}$).[37] Thus, differing from the situation for the short I blocks used in this study, $\tilde{G}_e^{(b)}$ may be significantly larger than $\tilde{G}_e^{(l,d)}$ for long I blocks.
(39) For SI/C_{14} and SB/C_{14} solutions at $T < T_{ODT}$, Yao et al.[22] found slow dielectric modes that are superficially similar to the dielectric modes of our SI/C_{14} solution (seen as the up-turn of ϵ'' in the plastic regime). Since the B blocks had no parallel dipoles and their global motion was dielectrically inert, the slow modes commonly seen for SI and SB were related to the domain structures.[22] Intensities of those modes were found to *decrease* with increasing T.[22] This feature is in contrast to that of the slow modes (up-turn of ϵ'') of our SI/C_{14} system. Thus, the slow dielectric modes appear to have different origins for our systems (having $\cong$ 30/70 S/I composition) and the systems examined by Yao et al.[22] (having $\cong$ 50/50 S/I or S/B composition).
(40) (a) An additional, interesting possibility considered by Morrison et al.[40b] is the conversion of the bridges to loops during (plastic) flow. The tension acting along the bridges under flow may destabilize the bridge conformation and increase the loop population. Turner[40c] carried out theoretical analyses for this type of bridge−loop conversion. If this conversion takes place in our SIIS systems, the number of bridges pulling out the S blocks is reduced and the flow-induced dielectric changes becomes smaller. (b) Morrison, F. A.; Mays, J. W.; Muthukumar, M.; Nakatani, A. I.; Han, C. C. *Macromolecules* **1993**, *26*, 5271. (c) Turner, M. S. *Macromolecules* **1995**, *28*, 6878.
(41) $\tilde{\sigma}_y^{(b)}$ and $\tilde{\sigma}_y^{(l,i)}$ of the bridges and interdigitated loops are determined by the mixing barrier for the S and I blocks. This barrier is larger for longer blocks. Thus, at a given T, the contribution of the bridges and interdigitated loops to σ_y would be enhanced with increasing molecular weights of the S and I blocks.

MA9617577